

1 **Deglacial history of the Pensacola Mountains, Antarctica from glacial geomorphology and cosmogenic** 2 **nuclide surface exposure dating**

3
4 Bentley, M.J.¹, Hein, A.S.², Sugden, D.E.², Whitehouse, P.L.¹, Shanks, R.³, Xu, S.³, Freeman, S.P.H.³

5
6 ¹Department of Geography, Durham University, Lower Mountjoy, South Rd, Durham, DH1 3LE, UK

7 ²School of Geosciences, University of Edinburgh, Drummond St, Edinburgh, EH8 9XP, UK

8 ³AMS Laboratory, Scottish Universities Environmental Research Centre, Scottish Enterprise Technology
9 Park, East Kilbride, G75 0QF, UK

12 **Abstract**

13 The retreat history of the Antarctic Ice Sheet is important for understanding rapid deglaciation, as well as to
14 constrain numerical ice sheet models and ice loading models required for glacial isostatic adjustment
15 modelling. There is particular debate about the extent of grounded ice in the Weddell Sea embayment at
16 the Last Glacial Maximum, and its subsequent deglacial history. Here we provide a new dataset of
17 geomorphological observations and cosmogenic nuclide surface exposure ages of erratic samples that
18 constrain the deglacial history of the Pensacola Mountains, adjacent to the present day Foundation Ice
19 Stream and Academy Glacier in the southern Weddell Sea embayment. We show there is evidence of at
20 least two glaciations, the first of which was relatively old and warm-based, and a more recent cold-based
21 glaciation. During the most recent glaciation ice thickened by at least 450 m in the Williams Hills and at
22 least 380 m on Mt Bragg. Progressive thinning from these sites was well underway by 10 ka BP and ice
23 reached present levels by 2.5 ka BP, and is broadly similar to the relatively modest thinning histories in the
24 southern Ellsworth Mountains. The thinning history is consistent with, but does not mandate, a Late
25 Holocene retreat of the grounding line to a smaller-than-present configuration, as has been recently
26 hypothesized based on ice sheet and glacial isostatic modelling. The data also show that clasts with
27 complex exposure histories are pervasive and that clast recycling is highly site-dependent. These new data
28 provide constraints on a reconstruction of the retreat history of the formerly-expanded Foundation Ice
29 Stream, derived using a numerical flowband model.

31 **Background and rationale**

32 The Antarctic Ice Sheet is the largest potential contributor to future sea-level rise. It is currently losing mass
33 (King et al., 2012; Shepherd et al., 2012) and some studies suggest that the rate of mass loss is accelerating
34 (Harig and Simons, 2015; Velicogna et al., 2014; Williams et al., 2014). Understanding the past history of the
35 ice sheet is important because: it can inform how the ice sheet has responded to past environmental

36 changes, and record its trajectory preceding the observational record; it allows us to test ice sheet models
37 by hindcasting; and it provides us with inputs for models of glacial isostatic adjustment (GIA) , which are
38 needed to interpret satellite gravimetric measurements of ice mass loss (Bentley, 2010).

39

40 The Weddell Sea sector of the ice sheet has not seen the same level of attention as other areas such as the
41 Amundsen Sea and Ross Sea. This is despite some studies suggesting that the area is particularly susceptible
42 to ice shelf thinning (Hellmer et al., 2012) and grounding line retreat (Ross et al., 2012; Wright et al., 2014).
43 Part of this sensitivity derives from the fact that the southern part of the area is overdeepened, particularly
44 in the east, where several subglacial basins are comparable in depth to other deep but grounded parts of
45 the West Antarctic Ice Sheet, for example, along the Amundsen Sea coast. The largest trough in the
46 Weddell Sea, the Foundation-Thiel Trough, is 1300-1500 m deep and extends north-south for >1000 km,
47 right across the Weddell Sea continental shelf to the shelf break (Fig. 1). Its position, size and extent mean
48 that it was once occupied by a major ice stream (the “Thiel Trough Ice Stream”) draining ice through an
49 area east of Berkner Island. This ice stream is likely to have exerted a key control on regional ice elevation.

50

51 At present there are two alternative models for the Last Glacial Maximum (LGM) extent of ice in the
52 Weddell Sea embayment (Bentley et al., 2014; Hillenbrand et al., 2014). The first, based largely on marine
53 geological evidence is an extensive model with ice grounded over the outer continental shelf (Hillenbrand
54 et al., 2012; Larter et al., 2012). The implication of this model is that the Thiel Trough Ice Stream would be
55 grounded as far as the shelf break. The second, based largely on terrestrial evidence of minor elevational
56 change of the ice sheet at the LGM (Bentley et al., 2010; Hein et al., 2011; Mulvaney et al., 2007) is a
57 restricted model with the grounding line of the Thiel Trough Ice Stream confined to the mid- to inner-shelf
58 (Bentley et al., 2010; Hillenbrand et al., 2014; Le Brocq et al., 2011; Whitehouse et al., 2012).

59

60 In addition to the debate on ice sheet extent, the timing of post-glacial thinning in the Weddell Sea is not
61 yet well understood. This hampers the development of ice loading models for GIA modelling, and the
62 understanding of recent (Late Holocene) change in the region. For example, although most studies have
63 assumed a simple retreat from LGM to present, a recent study has demonstrated that a Late Holocene re-
64 advance of the ice sheet may explain some formerly puzzling observations from GPS and glaciological
65 surveys (Bradley et al., 2015). Such a readvance has important implications for our understanding of ice
66 sheet stability, in that it implies that some grounding lines on inward dipping bedrock beds may be
67 advancing (Bradley et al., 2015). Such ‘unstable advance’ has been suggested on theoretical grounds
68 (Schoof, 2007). We require further observational data on ice sheet retreat timing to test the validity of such
69 ideas.

70

71 Our aim in this paper is to determine former ice sheet extent and elevation change adjacent to the
72 southern extension of the Thiel Trough Ice Stream (Fig. 1). The glacial geology of this area contains a record
73 of ice thickness change that can yield information on the extent of ice along the Foundation-Thiel Trough,
74 and the timing of its thinning from the local last glacial maximum (LLGM) (Clark et al., 2009) to its present
75 configuration. This paper describes the geomorphological evidence of former thicker ice levels in the
76 northern Pensacola Mountains and then provides a chronology of deglacial ice sheet thinning using
77 cosmogenic nuclide surface exposure dating. We also compare our results to a study of similar sites in the
78 Pensacola Mountains (Balco et al., 2016). A companion paper to this one (Whitehouse et al., submitted)
79 uses a glaciological model to explore the implications of the data presented both here and in Balco *et al.*
80 (2016) with regard to the former extent of ice in the Foundation-Thiel Trough.

81

82 **Study area and Methods**

83 The study area is the northern Pensacola Mountains, located at the southern extension of the Foundation-
84 Thiel Trough (Fig. 1). The Pensacola Mountains are split into the Neptune Range in the north, and the
85 Patuxent Range in the south. The Foundation Ice Stream, fed by the tributary Academy Glacier, flows south
86 to north through the area and becomes afloat immediately adjacent to the Schmidt Hills. The Foundation
87 Ice Stream is by far the largest West Antarctic Ice Sheet outlet in the south-eastern Weddell Sea:
88 indeed today it contributes more ice to the Weddell embayment than any other outlet except the
89 Evans Ice Stream (Joughin and Bamber, 2005). The margins of the Academy Glacier and Foundation Ice
90 Stream have several blue-ice areas with abundant supraglacial morainic debris, and this coupled to the
91 presence of numerous nunataks along their flanks means that there is a rich record of past ice sheet
92 elevational changes preserved.

93

94 We studied the geomorphology and sampled altitudinal transects of erratic sandstone clasts at several
95 sites: Schmidt Hills, Williams Hills, Mt. Bragg and Mt. Harper, and Thomas Hills (Fig. 1, Fig. 2.). Striation
96 directions are corrected to true north using declination values that vary across the study area from 23 to
97 31° east of north.

98

99 **Sampling of erratics and cosmogenic nuclide analysis**

100 The geology of the Pensacola Mountains is dominated by quartz-bearing lithologies: dominantly a mix of
101 folded sandstones, mudstones, conglomerates and limestones, with a more minor series of lava flows and
102 pillow lavas in the western part (Schmidt et al., 1978) and so a large proportion of erratics are suitable for
103 exposure dating using ^{10}Be and ^{26}Al contained in quartz. The presence of abundant erratics left behind by a
104 thinning ice sheet was noted by Schmidt *et al.* (1978) who described erratics on 'most rock slopes' up to
105 1000 m above present day ice. Erratic samples were taken whole or sampled from larger boulders with a

106 hammer and chisel. Our particular focus was in understanding the deglacial (thinning) history of the
107 different areas studied and we sampled erratics along altitudinal transects for this reason. The sampling
108 strategy for cosmogenic nuclides was designed to reduce the chance of nuclide inheritance, and exclude
109 the possibility of nuclide loss through erosion. Specifically, we sampled erratics that were perched on
110 bedrock, felsenmeer or drift surfaces, and avoided any samples that were embedded in drift, or sitting at
111 the base of slopes in order to minimise problems of post-depositional movement and self-shielding.
112 Because our focus is on the most recent deglacial thinning we selected the freshest erratics, and so avoided
113 erratics with weathering such as ventification, tafoni, spallation, weathering rinds or patina. We targeted
114 sub-glacially derived clasts with striated surfaces and sub-angular to sub-rounded shapes. Topographic
115 shielding was measured using an abney level and compass.

116

117 The sample and cosmogenic nuclide data are presented in Tables 1-2, and Figure 2. All exposure ages
118 discussed are based on ^{10}Be ages because the production rate is better constrained; ^{26}Al was used to
119 provide a check on a range of selected samples from different sites and in particular to determine, within
120 the errors of the approach, that the younger ages were concordant within error - and therefore less likely
121 to be reworked. In the case of the older ages (>100 ka) we used ^{26}Al analysis of a sub-set of samples to
122 determine whether they had experienced periods of burial, and were therefore more likely to record
123 complex exposure histories or reworking over more than one interval of ice sheet thickening and thinning.

124

125 **Laboratory and analytical techniques**

126 Whole rock samples were crushed and sieved to obtain the 250-710 μm fraction. Be and Al were
127 selectively extracted from the quartz component of the whole-rock sample at the University of Edinburgh's
128 Cosmogenic Nuclide Laboratory following established methods (Bierman et al., 2002; Kohl and Nishiizumi,
129 1992). $^{10}\text{Be}/^9\text{Be}$ and $^{26}\text{Al}/^{27}\text{Al}$ ratios were measured in 20 – 30 g of quartz at the Scottish Universities
130 Environmental Research Centre (SUERC) Accelerator Mass Spectrometry (AMS) Laboratory in East Kilbride,
131 UK. Measurements are normalised to the NIST SRM-4325 Be standard material with a revised (Nishiizumi
132 et al., 2007) nominal $^{10}\text{Be}/^9\text{Be}$ of 2.79×10^{-11} , and the Purdue Z92-0222 Al standard material with a nominal
133 $^{26}\text{Al}/^{27}\text{Al}$ of 4.11×10^{-11} , which agrees with the Al standard material of Nishiizumi (2004) with half-life of
134 0.705 Ma (Xu et al., 2010). SUERC ^{10}Be -AMS is insensitive to ^{10}B interference (Xu et al., 2013) and the
135 interferences to ^{26}Al detection are well characterised (Xu et al., 2014). Process blanks ($n = 19$) and samples
136 were both spiked with 250 μg ^9Be carrier (Scharlau Be carrier, 1000 mg/l, density 1.02 g/ml). Blanks were
137 spiked with 1.5 mg ^{27}Al carrier (Fischer Al carrier, 1000 ppm) and samples were spiked with up to 1.5 mg
138 ^{27}Al carrier (the latter value varied depending on the native Al-content of the sample). Blanks range from 5
139 $\times 10^{-15}$ – 3×10^{-14} [$^{10}\text{Be}/^9\text{Be}$] (less than 5% of total ^{10}Be atoms in all but the youngest samples); and 2×10^{-15} –
140 2×10^{-14} [$^{26}\text{Al}/^{27}\text{Al}$] (less than 2% of total ^{26}Al atoms in all but the youngest samples). Concentrations in

141 Table 1 are corrected for process blanks; uncertainties include propagated AMS sample/lab-blank
142 uncertainty, a 2% carrier mass uncertainty, and a 3% stable ^{27}Al measurement (ICP-OES) uncertainty.

143

144 **Exposure age calculations**

145 For exposure age calculations we used default settings in Version 2.0 of the CRONUScalc programme
146 (Marrero et al., 2015). The CRONUS-Earth production rates (Borchers et al., 2015) with the nuclide-
147 dependent scaling of Lifton-Sato-Dunai (Lifton et al., 2014) were used to calculate the ages presented in the
148 paper. Sea level and high latitude production rates are 3.92 ± 0.31 atoms $\text{g}^{-1}\text{a}^{-1}$ for ^{10}Be and 28.5 ± 3.1
149 atoms $\text{g}^{-1}\text{a}^{-1}$ for ^{26}Al . The alternative use of Lal/Stone (Lal, 1991; Stone, 2000) scaling does not change the
150 conclusions of the paper despite the approximately 3% and 6% older exposure ages for ^{10}Be and ^{26}Al ,
151 respectively. Rock density is assumed 2.7 g cm^{-3} and the attenuation length used is $153 \pm 10 \text{ g cm}^{-2}$. No
152 corrections are made for rock surface erosion or snow cover and thus exposure ages are minima. Finally,
153 we make no attempt to account for the relatively minor production-rate variations that would be caused by
154 elevation changes associated with glacial isostatic adjustment of the massif through time (Stone, 2000;
155 Saganuma et al., 2014). All ages are apparent exposure ages, which make the assumption that all exposure
156 has been achieved in a single episode at the current location of the sample, and that the sample has not
157 been covered by snow or sediment, and has experienced zero erosion.

158

159 **Results**

160 From the sediments, moraines and erosional landforms preserved in the Neptune and Patuxent Ranges we
161 have identified evidence for ice sheet expansion (thickening) and retreat (thinning). The area shows
162 abundant evidence of thicker ice, with sandstone erratics strewn over most surfaces visited (Fig. 3a). A
163 small number of features provide evidence of former ice limits (e.g., Fig. 3b), and in some cases show
164 complex and repeated interaction of different ice masses (Fig. 3c). In all cases we sampled erratics over
165 altitudinal profiles from the highest summits to the present ice margin. The exposure ages of these erratics
166 yields a thinning history for the Foundation Ice Stream and Academy Glacier, which is presented after a
167 description of the glacial geomorphology of the sample sites.

168

169 **Geomorphology**

170 The erratic lithologies in the Neptune Range are dominated by Dover Sandstone (white to yellow, medium
171 to coarse-grained, finely bedded to massive, quartz-rich) (Schmidt et al., 1978). Erratics are found on at
172 least the lower parts of almost every nunatak visited, and in many cases are abundant. There are fewer
173 Dover Sandstone erratics on nunataks in the Patuxent Range: here erratic lithologies tended to be darker-
174 coloured, harder and finer-grained sandstones. Although not generally sampled, other erratic lithologies
175 seen on nunataks include sandstone with conglomeratic layers (including granodiorite pebbles), basalt

176 (fine-grained, weathered, rounded, ventifacted), dolerite-gabbro (coarse, angular blocks), granodiorite
177 (pebble and small cobbles only), granite, gneiss and limestone. Some sandstone erratics show one or more
178 of granular disaggregation, spalling and tafoni. Whilst overall across the study area the erratics are of
179 diverse lithologies, we focused sampling on the Dover Sandstone clasts as they were the commonest clasts
180 at most localities and had a fresher appearance than some of the basalt (ventifacted) or other sandstone
181 (tafoni weathering) clasts. A few Dover Sandstone clasts had a darker yellow weathered outer surface;
182 these were avoided in sampling.

183

184 Many of the slopes in the area are mantled by a veneer of debris, much of it made up of a layer (> 30 cm
185 thick) of pale yellow-brown (fresh) to khaki brown (weathered) silty diamict, with locally-derived clasts, and
186 open pore spaces up to a few mm across. The diamict has a hard crust and is also partially-cemented.
187 Surface salt encrustation of this diamict is common. Some slopes have small terraces, 2-4 m across with
188 risers of 30-50 cm. Exposures of the diamict are common in these risers or in frost cracks that cut through
189 the terracing. Such features are particularly common downslope of snow patches, probably due to
190 availability of liquid water. This diamict underlies talus slopes, desert pavement cover and many of the
191 erratics sampled by us, but it is not ubiquitous and some of the nunataks, especially in the Schmidt Hills and
192 parts of the Thomas Hills, do not have exposures of a diamict. In these locations there is a felsenmeer of
193 locally-derived bedrock on low-angle slopes.

194

195 Many nunataks have areas of striated bedrock. For example, in Williams Hills, the bedrock on Pillow Knob
196 (NE end) is well-striated with two generations of striations. The first is finely-spaced, mm-scale, regular and
197 extends across bedrock surfaces for 10s of cm (Fig. 3d). These have a distinct weathering sheen or patina
198 over the surface. Their trend is 050-230°. These striations are found commonly on surfaces all over the
199 upper ridge and on the summit. The second, cross-cutting set of striations are irregular, cm-scale 'gouges'
200 (up to 1 cm wide, but usually 2-5 mm wide) that cut into the weathering patina, and are oriented
201 approximately 100-280°. They incise (1-2 mm) the patina and are themselves not weathered (Fig. 3d).
202 These gouges are not continuous (unlike the earlier striation set) and can be identified as individual gouges
203 up to 12-15 cm long, but usually only up to 5 cm. We follow Atkins *et al.* (2002) and Bentley *et al.* (2006) in
204 interpreting the two sets of striations as evidence for an early warm-based ice sheet (closely-spaced,
205 polished, weathered striations) followed by a later cold-based ice sheet (unweathered, less regular gouges).
206 However, at one location on the NE side of Pillow Knob both sets appear more closely-spaced, regular and
207 equally weathered, and so we cannot rule out that the second ice sheet was warm-based, at least in parts.

208

209 Bedrock throughout the area is usually weathered with a dark red surface patina. Locally-derived talus is
210 common on steeper slopes and in places this overlies either the bedrock or the silty diamict. Both the
211 weathered bedrock and the silty diamict extend right down to the present ice surface.

212

213 **SCHMIDT HILLS**

214 The Schmidt Hills are a line of nunataks along the east side of the Foundation Ice Stream, close to its
215 grounding line (Fig 2a). Spurs from these nunataks extend west down to the ice margin, at ~200-300 m asl.
216 Erratics are rare on all nunataks in the Schmidt Hills. For example on Dimmo Peak, only two true erratics
217 (one sandstone, one granitic) were found in the 400 m elevational range between the ice edge on the SE
218 side of the nunatak and the summit, and both were found at a relatively low elevation. At ~860 m on the W
219 ridge of Mt. Nervo there is a local concentration of sandstone and conglomerate erratics that are of
220 sufficient lithological and colour/weathering diversity for us to be confident that they are not originally
221 derived from a single clast.

222

223 No striations were found on summits and virtually all the bedrock surfaces have weathered surfaces (Fig.
224 3e). Lower down (below ~ 600 m asl) there are many striated surfaces on a spur W of Dimmo Peak, with
225 trend 036-216 to 056-236°. Lower parts of the spurs in Schmidt Hills also appear more rounded than the
226 summits. Diamict occurs over parts of the nunataks but is more commonly exposed on the lower spurs,
227 where the debris cover is modified by surficial mass movement. In several locations on the S side of Mt.
228 Nervo (e.g., 83° 14.494 S, 057° 56.440 W, 975 m) there are bedrock fractures that have been filled by
229 diamict.

230

231 The degree of weathering increases upwards on Mt. Nervo and Mt. Coulter such that near the summits
232 there are features such as tafoni weathering, spalling, and thick weathering rinds. The ridge crests
233 themselves are weathered such that cleaved sedimentary bedrock forms soft friable surfaces, whilst basalts
234 have weathered into nodules. Bowl-shaped depressions a few 100m across on the flanks of these nunataks
235 contain extensive periglacial (polygons, stripes, terraces, deep frost cracks) deposits containing pale
236 yellow silty diamict, >30 cm thick. At the mouth of the bowl on the SW flank of Mt. Nervo there are
237 prominent morainic deposits forming a mantle of debris over linear bedrock features sub-parallel to the
238 Foundation Ice Stream margin.

239

240 **WILLIAMS HILLS**

241 The Williams Hills have abundant erratics at all elevations, lying on the yellow silty diamict, on felsenmeer,
242 on summit plateaux, or on bedrock (Fig. 2b). The vast majority of these are erratics of Dover sandstone.
243 There is also evidence of ice transport of local lithologies (translocation of clasts from host outcrops on flat
244 surfaces or uphill). Weathered, pervasively striated bedrock shows 'old' overriding (warm-based)
245 glaciations trending 035-215° (Mt. Hobbs) or 050-230° (Pillow Knob). Fresher striations trend 100-280° and
246 are scattered and more gouge-like (cold-based). The yellow diamict is ubiquitous over all surfaces, from the
247 modern ice edge to the highest summit (Mt. Hobbs).

248

249 **MT. HARPER AND MT. BRAGG**

250 Along the northern margin of the Academy Glacier there are a series of nunataks that have a geological
251 record of glacier fluctuations on their southern flanks. The westernmost of these is Mt. Harper, with Mt.
252 Bragg to the east (Fig. 2c). There are extensive blue ice areas with supraglacial moraines along this margin
253 of the Academy Glacier.

254

255 Mt. Harper has a series of low knolls directly south of the main nunatak. These are mantled in a veneer of
256 drift that is composed mainly of the local basaltic lithology but with abundant freshly weathered sandstone
257 clasts. There is an underlying sandy diamict present but this is generally confined to pockets in bedrock.

258

259 The most prominent glacial feature on Mt. Bragg is a distinctive line of boulders located about 200m above
260 the present ice surface and which can be traced wrapping continuously around the slopes of Mt. Bragg for
261 up to 2 km (Fig. 3b). The boulder moraine is composed of off-white to yellow erratics. To the east (up-ice) it
262 cannot be traced beyond a talus slope directly below the summit of Mt. Bragg. To the west (down-ice) the
263 limit descends parallel to the modern glacier margin below. There is no apparent difference in weathering
264 of bedrock on either side of the boulder limit, and a small number of fresh sandstone erratics are found on
265 the slopes immediately above it. Bedrock on Mt. Bragg has a reddish-brown to purple weathering sheen,
266 and in places has polish and striations. The striations are mm-scale, finely-spaced, trend 077-257° and are
267 widely distributed.

268

269 Higher up, the west summit (1200 m) of Mt. Bragg is highly weathered with an orange-brown patina and
270 ubiquitous frost-shattering of bedrock. The number of erratics mantling the surface is much less than lower
271 on the nunatak, and the erratics themselves are more weathered than those lower down. In particular
272 volcanic erratic clasts have polish, weathering patina and ventifaction.

273

274 On the south side of the Academy Glacier we sampled former lake shorelines in the Mt. Lowry region: these
275 may record ice sheet thinning (see Hodgson and Bentley (2013) for full description). The lake shorelines are
276 covered by sub-fossil microbial mats that have desiccated into grey papery deposits that are found
277 preserved under cobbles and boulders.

278

279 **THOMAS HILLS**

280 The Thomas Hills comprise a series of NW-SE trending ridges that flank the east side of the Foundation Ice
281 Stream, upstream of its confluence with the Academy Glacier (Fig. 2d). Here we report the geomorphology
282 from the spurs¹ of Mt. Yarborough, Sugden Ridge, Clapperton Ridge, and Bentley Peak.

283

284 **Mt. Yarborough**

285 Mt. Yarborough sits towards the SW end of the Thomas Hills. Most of the nunatak is mantled in morainic
286 debris and numerous erratics. Striations near the summit of Mt. Yarborough and close to the ice margin
287 trend 119-299°, and lower slopes are mantled in a silty white diamict. Erratics are numerous and were
288 sampled from the summit down to the edge of the Foundation Ice Stream.

289

290 **Sugden Ridge**

291 The glacial geomorphology preserved on this ridge records the interaction between the Foundation Ice
292 Stream and more locally-sourced ice spilling over from the MacNamara Glacier to the south-east. The
293 Foundation Ice Stream is higher than the area between the spurs of the Thomas Hills and so lobes of the
294 Foundation Ice Stream flow downhill into the embayments, each of them terminating in an area of blue-ice,
295 and hence net ablation. At the northern end of the ridge there is a small lobe of Foundation Ice Stream ice
296 that flows down to the SE into the valley between Sugden and Clapperton Ridges, and former positions of
297 this lobe are marked by a series of lateral moraines on the NE flank of Sugden Ridge. Each of these
298 moraines consists of distinct lines of pale sandstone boulders, except for the lowest moraine close to the
299 present Foundation Ice Stream margin, which constitutes a substantial ridge of diamict a few metres high.
300 The moraines range in elevation from just a few metres above the present ice margin (370 m asl) to 150 m
301 above the present ice, and have gradients consistent with formerly expanded Foundation Ice Stream ice.
302 Similarly, former positions of a lobe derived from the MacNamara Glacier that spilled over the col between
303 the two ridges and flowed NW towards the Foundation Ice Stream are also recorded on the same slope.
304 Some of these moraine sequences intersect and overlap (Fig. 3c). Finally there is an area of patterned
305 ground – probably representing former snowpatches – that descends NE-wards from the middle of the
306 ridge forming Sugden Ridge (Fig. 3c). The northern ridge summit above the moraines is striated whilst the
307 southern parts of the ridge are mantled in silty diamict with a widespread surface salt encrustation.

308

309 **Clapperton Ridge**

310 The sandstone bedrock of Clapperton Ridge is deeply weathered, striated in places and an overlying silty
311 diamict is widespread, including overlying striated bedrock. Striations in a col on the ridge trend 129-309°,
312 and are of the extensive, finely-spaced (warm-based) type. No scattered striations or gouges (cold-based)
313 were seen cutting them.

¹ Only a few of the spurs in the Thomas Hills are named on the 1960s USGS map and so in 2011 the UK Antarctic Place Names Committee named the previously un-named spurs.

314

315 **Bentley Peak**

316 This minor peak lies at the NE end of Thomas Hills. Striae are visible at all altitudes on this nunatak, and
317 trend 130-310°. We sampled a transect of erratics and quartz bedrock veins from the summit (715 m) down
318 to the Foundation Ice Stream margin at 490 m. The lowest part of the nunatak is mantled in a thick diamict
319 that has an unweathered appearance and contains fresh, unweathered erratics.

320

321 **GEOMORPHOLOGICAL INTERPRETATION**

322 There is a consistent pattern of glacial geomorphology in the Pensacola Mountains. Specifically there is
323 evidence of at least two major glacial phases or configurations: the first of these was a warm-based
324 glaciation that striated bedrock across the field area and flowed oblique to present-day ice flow. For
325 example, in the Williams Hills, modern ice flow is northwards, but striations show former flow aligned NE-
326 SW. This may have been the same glacial phase that deposited a near-ubiquitous silty yellow diamict across
327 the field area and which occurs directly over many of the striated surfaces. The weathering of the striated
328 surfaces and of the diamict itself suggests that this glaciation was old, and we cannot rule out that the
329 diamict is an equivalent of the Sirius Group diamictictons or other several-million year old diamicts found
330 elsewhere in the Transantarctic Mountains. A second glacial phase constituted a cold-based ice sheet
331 expansion that over-rode and striated several summits, for example, in the Williams Hills. There is little
332 other evidence of erosion, and ice flowed obliquely to the earlier phase. This second phase is associated
333 with the deposition of erratics across almost all surfaces, as well as a fresh diamict in a few places. Thinning
334 from this glaciation left boulder moraines recording former ice margins along the side of Mt. Bragg and
335 Thomas Hills, and erratics located from summits to present ice elevations. During this period, there were
336 interactions between an expanded Foundation Ice Stream/Academy Glacier and more locally-sourced ice,
337 such as is recorded in the Thomas Hills.

338

339 The Schmidt Hills are anomalous in this regional pattern in that they contain few erratics. Where they do
340 occur they tend to cluster in highly localized concentrations, such as on the W ridge of Mt. Nervo. In the
341 Schmidt Hills and in some of the Thomas Hills there is a consistent pattern of summits being significantly
342 more weathered than lower reaches.

343

344 **COSMOGENIC NUCLIDE EXPOSURE AGES**

345 We sampled and analysed 105 erratics to derive their exposure ages using cosmogenic nuclides. The
346 exposure ages ranged from 2.5 ka to 3 Ma but with significant clustering of ages < 10 ka. When plotted
347 against their height above present day ice the younger ages in two of the four areas studied show clear
348 thinning trajectories in the Holocene (Table 2, Fig. 4): Williams Hills and the closely adjacent sites of Mt.
349 Bragg and Mt. Harper. Other sites show more complex histories of ice sheet fluctuations (Fig. 4). In all four

350 areas the analysed samples include a component of older material, a common feature of cosmogenic
351 isotope-derived chronologies of ice sheet thinning in Antarctica (Balco, 2011; Balco et al., 2016; Bentley et
352 al., 2006; Bentley et al., 2010; Hein et al., 2011, 2014; Mackintosh et al., 2011) caused by individual clasts
353 being recycled or overridden during ice sheet thickening-thinning cycles. In the case of the subset of older
354 samples analysed for ^{26}Al these all yielded discordant ages implying a complex exposure history with at
355 least one period of burial.

356

357 *Schmidt Hills*

358 In the Schmidt Hills, of the eight erratic samples analysed, there are no samples younger than 236 ka, and
359 most are substantially older, up to 3 Ma (Fig. 4a). Whilst there may be a partial record of fluctuations over
360 successive glacial cycles the site does not provide any constraints on deglaciation from the LLGM.

361

362 *Williams Hills:*

363 Of the 20 cosmogenic exposure dates 17 yield Holocene ages and show that thinning of the ice sheet
364 occurred from at least 450 m above present ice elevations. This thinning was progressive from the Early to
365 mid-Holocene and reached 50 m above present-day ice by 5 ka. Notably there are no samples younger than
366 5 ka (Fig. 4b, c).

367

368 *Mt. Bragg and Mt. Harper:*

369 We analysed 35 samples from Mt Bragg and Harper, and these range from 2.5 ka to 395 ka but with a
370 significant number, especially at Mt Harper, yielding Holocene ages. The data show that the ice sheet
371 thinned from at least 380 m above present ice with the majority of the samples deposited below 240 m
372 above present ice (Fig. 4d, e) from the early to mid-Holocene. Thinning may have been underway at 17.6 ka
373 but was certainly occurring progressively by 7.9 ka. The youngest age of 2.5 ka, close to present-day ice
374 shows that present ice levels were reached by 2.5 ka. Samples from the boulder moraine on the sides of
375 Mt. Bragg (~200 m above present ice) yielded a mixed population of ages (12, 37, 41, 74, 161, 206 ka).

376

377 *Thomas Hills*

378 The 42 samples analysed from several nunataks along the Thomas Hills yield a range of ages with the
379 majority dating from prior to the last glacial cycle, particularly on Mt. Yarborough and Clapperton Ridge
380 (Fig. 4g-j), including ages up to 953 ka. However, two sites, Sugden Ridge and Bentley Peak, have erratic
381 samples that yielded ages showing they were deposited during deglaciation from the Local Last Glacial
382 Maximum (Fig. 4g). For example, one Holocene sample with an age of 4.2 ka occurs at 125 m above present
383 ice on Bentley Peak, perched on fresh drift. This is consistent with the Bragg, Harper, and Williams massifs,
384 to which it is most closely located. However, all other samples from the flanks of this site yield ages
385 substantially older than the LGM and are likely reworked or have been preserved beneath ice. The ^{26}Al

386 exposure ages on a subset of samples show discordant ages, implying a complex exposure history, and thus
387 confirm this view of at least one period of burial.

388

389 *Sugden Ridge*

390 Sugden Ridge (Fig. 3c, Fig. 4g) yields a complex set of exposure ages on the cross-cutting moraines, and
391 does not provide a clear thinning history for the Foundation Ice Stream. Each moraine has yielded a
392 significant range of ages. The highest parts of Sugden Ridge yield pre-LGM exposure ages of 96 ka (peak)
393 and 563 ka (col). The highest Foundation Ice Stream moraine yields ages of 51.1 and 32.5 ka. It is notable
394 that all of the moraines below this yield mixed ages but that ages in the range 28 -33 ka occur in every
395 moraine. The most extensive and distinct moraine yields one age of 12.8 ka, which is the youngest age
396 anywhere on this spur. The lowest elevation moraine provides mixed ages between 380 and 28.7 ka.

397

398 **Discussion**

399 The data reported here show that the Foundation Ice Stream and its tributary Academy Glacier thickened
400 by 100s of metres during the LLGM. The data do not constrain the maximum thickening but it was >380-450
401 m close to the confluence of the Academy Glacier and the Foundation Ice Stream. The data do show
402 progressive thinning during the Holocene, and this is consistent with recent data from Balco *et al.* (2016)
403 that show similar thinning trajectories from the northern Pensacola Mountains (Fig. 3).

404

405 *Foundation Ice Stream and Academy Glacier thinning histories*

406 The most detailed thinning histories come from the north side of the Academy Glacier where the datasets
407 from Williams Hills and Mt. Bragg and Mt. Harper give similar, but not identical, deglacial trajectories (Fig.
408 4f) of progressive thinning from the early- to mid-Holocene. Specifically the Williams Hills data have no
409 samples younger than 5 ka whereas at Mt. Bragg and Mt. Harper there are younger samples. Moreover the
410 rate of thinning may have been faster at Williams Hills than at Mt. Bragg/Mt. Harper (Fig. 4b, d, f). Mt.
411 Hobbs, the highest summit of the Williams Hills, yielded an exposure age of 8.85 ka at 450 m above present
412 ice. On Mt. Bragg, the highest sample taken, 383 m above present ice, yielded an age of 17.6 ka. The data
413 do not directly constrain either the extent or timing of the maximum glaciation at either site.

414

415 The Williams Hills exposure ages are similar to the exposure ages reported from the same area by Balco *et al.*
416 (2016), which also show progressive thinning through the first half of the Holocene and no ages <4.18
417 ka. Figures 4b and 4f show that the thinning trajectories of the two datasets are closely coincident. Farther
418 south, in the Thomas Hills our data do not record a clear post-glacial thinning trajectory apart from a single
419 age of 4.2 ka at Bentley Peak and a single age of 12.8 ka amongst a mixed age population from a single
420 moraine on Sugden Ridge. However, the dataset from Balco *et al.* (2016) show that ice was >250 m thicker

421 at the southern end of the Thomas Hills in the early Holocene and that the ice thinned rapidly prior to 5 ka
422 (Fig. 4i), consistent with the sites along the north side of the Academy Glacier.

423

424 *Lack of recently exposed erratics in the Schmidt Hills*

425 The lack of erratics younger than 236 ka in the Schmidt Hills, despite widespread evidence for LGM
426 glaciation elsewhere in the Pensacola Mountains, is similar to the pattern found by Balco *et al.* (2016) from
427 the same area, where all of the ^{10}Be apparent exposure ages in the Schmidt Hills were from prior to the last
428 glacial cycle. Both our data and the data presented in Balco *et al.* (2016) show clear evidence for ice cover
429 up to 450 m thicker than present in the Williams Hills, which lie only a few 10 of kilometres south of the
430 Schmidt Hills (Fig. 1), and so this difference is puzzling. Balco *et al.* (2016) undertook multiple isotopic
431 analyses (^{10}Be , ^{21}Ne , ^3He , and ^{14}C) on their samples and showed that there were inconsistencies between
432 the different isotopes. They argued that although their *in situ* ^{14}C apparent exposure ages showed a clear
433 long-term exposure with no significant intervals of ice cover above 500 m elevation (corresponding to ice
434 ~350 m thicker than present), the dataset could not be reconciled with simple Holocene thinning histories.
435 They suggested that to explain the ages would require either significant unrecognized analytical errors (of
436 up to 25%), or a complex and unlikely configuration of LGM ice, which transported the samples from prior
437 exposure on higher summits in the Schmidt Hills. Balco *et al.* (2016) concluded that they could not clearly
438 resolve the exposure history of the Schmidt Hills but that the *in situ* ^{14}C concentrations were clear in
439 showing that any LGM ice cover of the area reached <500 m asl elevation.

440

441 We concur that the lack of dated evidence for LGM glaciation of the Schmidt Hills is difficult to explain.
442 Perhaps it reflects some effect of lithology on analytical procedures or more probably an effect of patterns
443 of local ice flow. It is notable that an expanded Childs Glacier, coming off the Iroquois plateau may have
444 diverted the debris-bearing ice that was flowing NW over the Williams Hills to the west before it reached
445 the Schmidt Hills (Fig. 1). The Balco *et al.* (2016) ^{14}C data require that the ice did not thicken more than
446 ~350 m above present at the Schmidt Hills. Given that the Foundation Ice Stream thickened at least by 450
447 m only a few tens of km to the south then this would require a significant steepening of the Foundation Ice
448 Stream gradient, or that the centreline of the Foundation Ice Stream thickened significantly more than the
449 margins at Schmidt Hills (Balco *et al.*, 2016). The implications of the Schmidt Hills data for former
450 configuration of an expanded Foundation Ice Stream are explored further using a numerical flowband
451 model in Whitehouse *et al.* (submitted), where it is demonstrated that differential thickening of the centre
452 and margins of the Foundation Ice Stream could potentially explain the Schmidt Hills data.

453

454 *Mixed age populations on boulder moraines and reworking of clasts*

455 Conventionally, boulder moraines provide a useful fix on the position of a formerly expanded ice margin
456 and rigorous dating of such a limit should yield a well-dated reconstruction of that margin. However, in the

457 Pensacola Mountains we found that each of the boulder moraines we mapped and sampled (Mt. Bragg,
458 Sugden Ridge) yielded mixed age populations. For this reason we have been unable to assign ages to any of
459 the boulder moraines. Each of these boulder limits is associated with a present-day ice margin that is
460 dominantly composed of blue-ice regions. The mixed ages imply that either the reworking of erratics along
461 the blue-ice margins of Foundation Ice Stream may be pervasive, or that the debris has been emerging at
462 the ice margin for millennia.

463

464 The cross-cutting moraines at Sugden Ridge reflect complex behaviour of the Foundation Ice Stream and
465 locally-sourced MacNamara Glacier. There are a number of features of the mixed age populations of these
466 moraines that are worthy of discussion. At face value, the mixed ages – ranging from 12.8 ka to 380 ka – are
467 difficult to reconcile with the Williams/Bragg/Harper trajectory of an expanded Foundation Ice Stream at
468 the LGM which thinned through the early to mid-Holocene. There are at least three possible explanations.
469 Firstly, all fluctuations at Sugden Ridge predate the LLGM and have then been over-ridden by thicker LLGM
470 ice. Overriding of landforms without modification by cold-based ice has been noted elsewhere in Antarctica
471 (Sugden et al., 2005). In this case the youngest age of 12.8 ka may be the closest representative thinning
472 age. Second, all fluctuations are post-LLGM but the majority of samples are reworked. This could explain
473 the substantial scatter on every moraine sampled. Third, the data may reflect the real timing of fluctuations
474 (dated by the youngest sample on each moraine) but would imply very small thickness changes at each site,
475 and also ice sheet thickening that is inconsistent with the timing of ice sheet change elsewhere in the study
476 area. The latter two explanations are very difficult to reconcile with the Bragg/Harper/Williams dataset and
477 with evidence of the Foundation Ice Stream thinning by 125 m since 4.18 ka at Bentley Peak, and so we
478 favour the first explanation, namely that the cross-cutting moraine sequences on Sugden Ridge have been
479 over-ridden.

480

481 *Comparison to other Weddell Sea deglacial chronologies*

482 Our data can be compared with previous work on the glacial history of the Antarctic Ice Sheet in the
483 Weddell Sea embayment. Bentley *et al.* (2010) showed modest LLGM thickening of 230-480 m in the
484 southern Ellsworth Mountains followed by progressive thinning through the Holocene to reach present ice
485 levels by c. 2 ka. This is similar to the glacial history reported here and both sites sit in similar configurations
486 close to the present-day grounding line where thickening is likely to have been significant during past
487 glacial periods. In the Shackleton Range, farther north along the Thiel Trough Ice Stream, Hein *et al.* (2011)
488 showed that there had been minimal thickening at the LGM. The implication of this is that an expanded
489 Thiel Trough Ice Stream could not have thickened significantly at the vicinity of the Shackleton Range (Hein
490 *et al.*, 2011; Hillenbrand *et al.*, 2014). Ice core data from Berkner Island showed that this ice rise, with a
491 current altitude of 886 m asl was not overridden by thick interior ice during the LGM and that it remained
492 an independent ice centre throughout the last glacial cycle (Matsuoka *et al.*, 2015; Mulvaney *et al.*, 2007).

493

494 *A Late Holocene ice sheet readvance in the Weddell Sea?*

495 Bradley *et al.* (2015) suggested that a number of puzzling glaciological and geophysical observations could
496 be explained if the ice sheet in the Weddell Sea had retreated to smaller-than-present-limits in the mid- to
497 Late Holocene and had subsequently advanced to its present configuration. Specifically, this would help
498 explain observations of grounding lines existing in an apparently stable configuration on reverse slopes, and
499 also low GPS-measured crustal uplift rates, including an observation of subsidence from at least one GPS
500 receiver located in the interior of the ice sheet inboard of the grounding line. Moreover, a readvance from
501 smaller-than-present would also explain the glaciological observations of significant Late Holocene flow re-
502 organisation of the Institute and Möller Ice Streams (Siegert *et al.*, 2013). Data from the Ellsworth
503 Mountains are consistent with the concept of a Late Holocene ice sheet readvance since the youngest
504 exposure ages of erratics close to the present margin are 2-3 thousand years old (Bentley *et al.*, 2010; Hein
505 *et al.*, 2016a). Our new data from the Foundation Ice Stream are consistent with the data from the
506 Ellsworth Mountains and glaciological observations from the Institute and Möller Ice Streams: specifically,
507 in the Williams Hills there are no exposure ages younger than 5ka (our data) or 4 ka (Balco *et al.*, 2016).
508 Thus the ice margin in the vicinity of the Williams Hills may have thinned below present ice levels any time
509 after 4ka, and only subsequently re-thickened. It is notable that the Williams Hills data show a very abrupt
510 lower limit to exposure ages and that the data would be consistent with rapid ice sheet thinning adjacent to
511 the Williams Hills at 4-5 ka. In the area of Mt. Bragg and Mt. Harper the youngest ages are slightly younger,
512 with the youngest age above the present margin being 3.1 ka (an age at the present margin yields 2.5 ka
513 but because it sits right at the present margin we cannot rule out it being reworked by the margin of a
514 thickening ice sheet). In summary, our data are consistent with, but do not mandate, a scenario of
515 Holocene thinning and subsequent thickening in the interval after 4 ka (Williams Hills) or 3.1-2.5 ka (Mt.
516 Bragg/Mt. Harper).

517

518 *Sampling of ice stream margins in Antarctica for thinning histories*

519 In Antarctica, blue ice regions are regions of net ablation, often due to sublimation under katabatic wind
520 regimes, in what would otherwise be the accumulation area of the ice sheet. They are a prime source of
521 glacially-deposited material because ablation brings englacial material to the ice sheet surface. . At face
522 value, this makes them attractive areas for sampling for studies of former thinning histories. However, the
523 problems of sampling for cosmogenic nuclide surface exposure dating from areas adjacent to blue ice
524 moraines have been apparent in several studies and this is no exception. In areas adjacent to blue ice on
525 the present-day Foundation Ice Stream or Academy Glacier, the apparent exposure ages we retrieved have
526 a high component of scatter (e.g., Mt. Bragg, Sugden Ridge, Mt. Yarborough). As in several previous studies,
527 the surface weathering characteristics or appearance of erratics cannot be used as a reliable guide to
528 relative age: fresh-looking erratics regularly yield 'old' ages (see discussion in Balco (2011) and Hein *et al.*

529 (2014)). Moreover, comparison of our work with that by Balco *et al.* (2016) shows that the proportion of
530 younger ages can change markedly in closely adjacent sites: for example in the Thomas Hills we sampled
531 Mt. Yarborough and found no samples younger than 255 ka (n=12), yet sampling by Balco *et al.* of the
532 adjacent nunataks on either side ('Nance Ridge' and 'South Mainland') yielded an age population where
533 50% of the ages were post-LGM in age (n=16). This implies significant variations in spatial distribution.

534

535 This problem of complex exposure ages in blue-ice regions also applies to distinct geomorphological limits
536 such as boulder moraines. Such a moraine can display a wide range of exposure ages, implying either
537 reworking of old clasts and/or a long period of stability during which boulders were deposited. In the
538 future, the complexity, once elaborated, holds potential for investigating the long-term stability of the ice
539 sheet (Ackert *et al.*, 2011; Hein *et al.*, 2016a; Hein *et al.*, 2016b).

540

541 Balco *et al.* (2016) tried the screening approach suggested by Ackert *et al.* (2007) whereby faster, cheaper
542 (but less accurate) ^3He analyses could be used to screen erratic populations for younger (post-LGM) clasts
543 in a mixed population. Unfortunately in the Pensacola Mountains the erratic lithologies possessed unusual
544 and variable He diffusion properties in quartz and so the ^3He analyses consistently underestimated
545 exposure ages. In fact, Balco *et al.* (2016) concluded that the ^3He analyses simply acted as a proxy for
546 diffusion properties of each lithology rather than any reliable measure of exposure age. *In situ* ^{14}C analyses
547 have been used successfully in a small number of glacial geologic studies in Antarctica and elsewhere to
548 test for clast recycling (e.g., White *et al.* (2011)). Balco *et al.* (2016) tried a similar approach in the Schmidt
549 Hills to look at the reworking problem but the results suggest that there may be previously unrecognised
550 analytical problems, and the data did not robustly constrain the reworking issue.

551

552 It is notable that in the Williams Hills - the area with least blue ice on the adjacent ice stream - both our
553 study and that of Balco *et al.* (2016) yielded robust and closely similar thinning trajectories for post-LGM ice
554 sheet behaviour. The implication is that recycling or inheritance is much less of a problem in this area and
555 that the erratics can provide a robust age-elevation array.

556

557 **Conclusions**

558 A new dataset of geomorphological and cosmogenic nuclide surface exposure dating from the Pensacola
559 Mountains allows us to make inferences on the deglacial history of this region, and in particular the
560 deglacial history of the Foundation Ice Stream.

- 561 1. There is evidence of at least two glacial configurations: early warm-based glaciation(s) that
562 weathering suggests was/were relatively old, and second, more recent cold-based glaciation(s).
- 563 2. The geomorphology of the area records a thinning history since the local Last Glacial Maximum

- 564 3. Thickening in the most recent glaciation was at least 450 m in Williams Hills and at least 380 m on
565 Mt. Bragg
- 566 4. The timing of the onset of thinning is not well-constrained by these data but was well underway by
567 the Early Holocene.
- 568 5. Cosmogenic isotopic data show that there was progressive thinning of the Foundation Ice Stream
569 and the tributary Academy Glacier between 10 and 2.5ka. The thinning trajectory is similar at
570 multiple sites: three sites on the flanks of the Foundation Ice Stream/Academy Glacier, from two
571 independent studies, show a consistent thinning history, reaching present ice levels by 2.5ka
- 572 6. Geomorphology and dating in the Thomas Hills shows thickening occurred, but has also revealed a
573 complex interaction between the Foundation Ice Stream margin and local ice. These fluctuations
574 are not yet well dated.
- 575 7. The modest thinning history reported here is broadly similar to that from the Ellsworth Mountains
576 (Bentley et al., 2010; Hein et al., 2016a).
- 577 8. The thinning history at this and other sites is consistent with, but does not mandate, a retreat of
578 the grounding line behind the present ice sheet margin followed by a Late Holocene readvance
579 (Bradley et al., 2015).
- 580 9. Clasts with complex exposure histories are pervasive, as in most blue ice areas of Antarctica, but
581 also highly variable over short distances.
- 582 10. These data provide constraints on attempts to infer former ice sheet extent in the Weddell Sea
583 using numerical flowband modelling of the former Thiel Trough Ice Stream (Whitehouse et al.,
584 submitted).
- 585

586 **Acknowledgements**

587 We thank the British Antarctic Survey pilots and operations staff who facilitated the work in the Pensacola
588 Mountains. Particular thank to James Wake for his assistance in the field. The work reported here forms
589 part of NERC grants NE/F014260/1, NE/F014252/1, and NE/F014228/1. We thank Greg Balco and a second,
590 anonymous reviewer for their comments, which improved the paper.

591

592 **List of Tables**

593

594 **Table 1.** Rock sample details and cosmogenic ^{10}Be and ^{26}Al concentrations in quartz-bearing
595 erratics.

596 *SS: sandstone; Qtz: quartz; Qtzite: quartzite; P. congl.: pebble conglomerate. Assumed rock
597 density 2.7 g cm^{-3} .

598 [†]AMS measurements made at Scottish Universities Environmental Research Centre (SUERC).

599 [§]Normalised to NIST SRM-4325 Be standard material with a revised nominal $^{10}\text{Be}/^9\text{Be}$ ratio ($2.79 \times$
600 10^{-11}) (Nishiizumi et al., 2007) and corrected for process blanks; uncertainties include propagated
601 AMS sample/lab-blank uncertainty and a 2% carrier mass uncertainty.

602 [#]Normalised to the Purdue Z92-0222 Al standard material with a nominal $^{27}\text{Al}/^{26}\text{Al}$ ratio of $4.11 \times$
603 10^{-11} that agrees with Al standard material of (Nishiizumi, 2004), and corrected for process blanks;
604 uncertainties include propagated AMS sample/lab-blank uncertainty and a 5% stable ^{27}Al
605 measurement (ICP-OES) uncertainty.

606

607 **Table 2.** Cosmogenic ^{10}Be and ^{26}Al surface exposure ages.

608 *Ages calculated with CRONUS-Earth CRONUScalc v.2.0 (Marrero et al., 2015), LSD scaling (Lifton
609 et al., 2014), no erosion correction; attenuation length $153 \pm 10 \text{ g cm}^{-2}$; ^{26}Al and ^{10}Be production
610 rates from CRONUS-Earth Project (Borchers et al., 2015).

611 [†](int) = Internal uncertainties; includes only concentration uncertainties based on lab/AMS
612 measurements. [†](ext) = External uncertainties; includes internal uncertainties plus scaling and
613 production rate uncertainties.

614 [†](full) = Full uncertainties; includes external uncertainties plus uncertainties on thickness (0.5 cm),
615 pressure (10 hPa), attenuation length (10 g cm^{-2}), and density (0.05 g cm^{-3}).

616 [^]Sample elevations are normalised to the elevation of the ice surface at the foot of the spur or
617 peak on which the sample lies, and so the plots in Figure 4 are in terms of elevation above present
618 ice.

619

620

621

622

623 **List of figures**

624 **Figure 1.** Location Map of the Pensacola Mountains study area, adjacent to the Foundation Ice
625 Stream and its tributary the Academy Glacier. Background is Landsat imagery from the LIMA
626 mosaic. Rock outcrop and grounding line are from Antarctic Digital Database. Bathymetry is from
627 BEDMAP2 (Fretwell et al., 2013). Inset shows location within the southern Weddell Sea
628 embayment. BI=Berkner Island; EM=Ellsworth Mountains; FTT=Filchner-Thiel Trough; IIS=Institute
629 Ice Stream; SR=Shackleton Range.

630
631 **Figure 2.** Field sites and sample locations. (a) Schmidt Hills, (b) Williams Hills, (c) Mt Bragg and Mt
632 Harper, (d) Thomas Hills. Background imagery in a and b is USGS Landsat 8 satellite imagery (Band
633 8). Background maps in c and d are the USGS 1:250,000 Reconnaissance Series Topographic Maps
634 of Antarctica (Sheets: SU21-25/13 (Schmidt Hills), SV21-30/1 (Gambacorta Peak) and SV11-20/4
635 (Thomas Hills). Place names proposed and adopted by the UK Committee on Antarctic Place
636 Names have been added. Cosmogenic nuclide sample locations are shown as green dots. See
637 Tables 1 and 2 for sample data.

638
639 **Figure 3.** Glacial geomorphology of the field area. (a) Erratic sandstone clasts on the Williams Hills,
640 (b) Boulder limit on south flank of Mt. Bragg, Academy Glacier visible below, (c) Panorama of
641 Sugden Ridge showing cross-cutting moraines: moraines deposited by an expanded Foundation Ice
642 Stream slope down from R to L and moraines from an expanded MacNamara Glacier slope down
643 from L to R. Red dots show samples, ^{10}Be ages in bold, and ^{26}Al ages in italics. Numbered black
644 dots show elevations (m asl). (d) Striations on Pillow Knob, Williams Hills. A set of weathered,
645 warm-based striations (parallel to compass-clinometer) are cut by a fresher set of cold-based
646 striations that incise the weathered surface, trending top right to bottom left. (e) Weathered
647 bedrock in the Schmidt Hills.

648
649 **Figure 4.** Thinning histories of sites in the Pensacola Mountains. (a) Schmidt Hills (all samples), (b)
650 Williams Hills (samples <20ka), (c) Williams Hills (all), (d) Mt. Bragg and Mt. Harper (<20 ka), (e)
651 Mt. Bragg and Mt. Harper (all), (f) Combined dataset of Williams Hills, Mt. Bragg and Mt. Harper
652 (<20ka), (g) Thomas Hills (Sugden Ridge, Clapperton Ridge, Bentley Peak) <50 ka, (h) Thomas Hills
653 (all), (i) Mt. Yarborough (<50 ka), (j) Mt. Yarborough (all). Data from this study as filled shapes,
654 data from Balco *et al.* (2016) are plotted as open circles.

655

656 References

- 657 Ackert, R.P., Jr., Mukhopadhyay, S., Pollard, D., DeConto, R.M., Putnam, A.E., Borns, H.W., Jr., 2011. West
658 Antarctic Ice Sheet elevations in the Ohio Range: Geologic constraints and ice sheet modeling prior to
659 the last highstand. *Earth Planet. Sci. Lett.* 307, 83-93.
- 660 Ackert, R.P., Mukhopadhyay, S., Parizek, B.R., Borns, H.W., 2007. Ice elevation near the West Antarctic Ice
661 Sheet divide during the Last Glaciation. *Geophys. Res. Lett.* 34.
- 662 Atkins, C.B., Barrett, P.J., Hicock, S.R., 2002. Cold glaciers erode and deposit: Evidence from Allan Hills,
663 Antarctica. *Geology* 30, 659-662.
- 664 Balco, G., 2011. Contributions and unrealized potential contributions of cosmogenic-nuclide exposure
665 dating to glacier chronology, 1990-2010. *Quat. Sci. Rev.* 30, 3-27.
- 666 Balco, G., Todd, C., Huybers, K., Campbell, S., Vermuelen, M., Hegland, M., Goehring, B.M., Hillebrand, T.R.,
667 2016. Cosmogenic-nuclide exposure ages from the Pensacola Mountains adjacent to the Foundation Ice
668 Stream, Antarctica. *Am. J. Sci.* 316.
- 669 Bentley, M.J., 2010. The Antarctic palaeo record and its role in improving predictions of future Antarctic Ice
670 Sheet change. *J. Quat. Sci.* 25, 5-18.
- 671 Bentley, M.J., Fogwill, C.J., Kubik, P.W., Sugden, D.E., 2006. Geomorphological evidence and cosmogenic Be-
672 10/Al-26 exposure ages for the Last Glacial Maximum and deglaciation of the Antarctic Peninsula Ice
673 Sheet. *Geol. Soc. Am. Bull.* 118, 1149-1159.
- 674 Bentley, M.J., Fogwill, C.J., Le Brocq, A.M., Hubbard, A.L., Sugden, D.E., Dunai, T.J., Freeman, S., 2010.
675 Deglacial history of the West Antarctic Ice Sheet in the Weddell Sea embayment: Constraints on past ice
676 volume change. *Geology* 38, 411-414.
- 677 Bentley, M.J., Ó Cofaigh, C., Anderson, J.B., Conway, H., Davies, B., Graham, A.G.C., Hillenbrand, C.-D.,
678 Hodgson, D.A., Jamieson, S.S.R., Larter, R.D., Mackintosh, A., Smith, J.A., Verleyen, E., Ackert, R.P., Bart,
679 P.J., Berg, S., Brunstein, D., Canals, M., Colhoun, E.A., Crosta, X., Dickens, W.A., Domack, E., Dowdeswell,
680 J.A., Dunbar, R., Ehrmann, W., Evans, J., Favier, V., Fink, D., Fogwill, C.J., Glasser, N.F., Gohl, K., Golledge,
681 N.R., Goodwin, I., Gore, D.B., Greenwood, S.L., Hall, B.L., Hall, K., Hedding, D.W., Hein, A.S., Hocking,
682 E.P., Jakobsson, M., Johnson, J.S., Jomelli, V., Jones, R.S., Klages, J.P., Kristoffersen, Y., Kuhn, G.,
683 Leventer, A., Licht, K., Lilly, K., Lindow, J., Livingstone, S.J., Massé, G., McGlone, M.S., McKay, R.M.,
684 Melles, M., Miura, H., Mulvaney, R., Nel, W., Nitsche, F.O., O'Brien, P.E., Post, A.L., Roberts, S.J.,
685 Saunders, K.M., Selkirk, P.M., Simms, A.R., Spiegel, C., Stollendorf, T.D., Sugden, D.E., van der Putten, N.,
686 van Ommen, T., Verfaillie, D., Vyverman, W., Wagner, B., White, D.A., Witus, A.E., Zwartz, D., 2014. A
687 community-based geological reconstruction of Antarctic Ice Sheet deglaciation since the Last Glacial
688 Maximum. *Quat. Sci. Rev.* 100, 1-9.
- 689 Bierman, P.R., Caffee, M.W., Davis, P.T., Marsella, K., Pavich, M., Colgan, P., Mickelson, D., Larsen, J., 2002.
690 Rates and timing of earth surface processes from in situ- produced cosmogenic Be-10, Beryllium:
691 Mineralogy, Petrology, And Geochemistry, pp. 147-205.
- 692 Borchers, B., Marrero, S., Balco, G., Caffee, M., Goehring, B., Lifton, N., Nishiizumi, K., Phillips, F., Schaefer,
693 J., Stone, J., 2015. Geological calibration of spallation production rates in the CRONUS-Earth project.
694 *Quat. Geochronol.*
- 695 Bradley, S.L., Hindmarsh, R.C.A., Whitehouse, P.L., Bentley, M.J., King, M.A., 2015. Low post-glacial rebound
696 rates in the Weddell Sea due to Late Holocene ice-sheet readvance. *Earth Planet. Sci. Lett.* 413, 79-89.
- 697 Clark, P.U., Dyke, A.S., Shakun, J.D., Carlson, A.E., Clark, J., Wohlfarth, B., Mitrovica, J.X., Hostetler, S.W.,
698 McCabe, A.M., 2009. The Last Glacial Maximum. *Science* 325, 710-714.
- 699 Fretwell, P., Pritchard, H.D., Vaughan, D.G., Bamber, J.L., Barrand, N.E., Bell, R., Bianchi, C., Bingham, R.G.,
700 Blankenship, D.D., Casassa, G., Catania, G., Callens, D., Conway, H., Cook, A.J., Corr, H.F.J., Damaske, D.,
701 Damm, V., Ferraccioli, F., Forsberg, R., Fujita, S., Gim, Y., Gogineni, P., Griggs, J.A., Hindmarsh, R.C.A.,
702 Holmlund, P., Holt, J.W., Jacobel, R.W., Jenkins, A., Jokat, W., Jordan, T., King, E.C., Kohler, J., Krabill, W.,
703 Riger-Kusk, M., Langley, K.A., Leitchenkov, G., Leuschen, C., Luyendyk, B.P., Matsuoka, K., Mouginot, J.,
704 Nitsche, F.O., Nogi, Y., Nost, O.A., Popov, S.V., Rignot, E., Rippon, D.M., Rivera, A., Roberts, J., Ross, N.,
705 Siegert, M.J., Smith, A.M., Steinhage, D., Studinger, M., Sun, B., Tinto, B.K., Welch, B.C., Wilson, D.,
706 Young, D.A., Xiangbin, C., Zirizzotti, A., 2013. Bedmap2: improved ice bed, surface and thickness datasets
707 for Antarctica. *Cryosphere* 7, 375-393.

708 Harig, C., Simons, F.J., 2015. Accelerated West Antarctic ice mass loss continues to outpace East Antarctic
709 gains. *Earth Planet. Sci. Lett.* 415, 134-141.

710 Hein, A.S., Fogwill, C.J., Sugden, D.E., Xu, S., 2011. Glacial/interglacial ice-stream stability in the Weddell Sea
711 embayment, Antarctica. *Earth Planet. Sci. Lett.* 307, 211-221.

712 Hein, A.S., Fogwill, C.J., Sugden, D.E., Xu, S., 2014. Geological scatter of cosmogenic-nuclide exposure ages
713 in the Shackleton Range, Antarctica: Implications for glacial history. *Quat. Geochronol.* 19, 52-66.

714 Hein, A.S., Marrero, S.M., Woodward, J., Dunning, S.A., Winter, K., Westoby, M.J., Freeman, S.P.H.T.,
715 Shanks, R.P., Sugden, D.E., 2016a. Mid-Holocene pulse of thinning in the Weddell Sea sector of the West
716 Antarctic Ice Sheet. *Nature Communications* 7.

717 Hein, A.S., Woodward, J., Marrero, S.M., Dunning, S.A., Steig, E.J., Freeman, S.P.H.T., Stuart, F.M., Winter,
718 K., Westoby, M.J., Sugden, D.E., 2016b. Evidence for the stability of the West Antarctic Ice Sheet divide
719 for 1.4 million years. *Nat Commun* 7.

720 Hellmer, H.H., Kauker, F., Timmermann, R., Determann, J., Rae, J., 2012. Twenty-first-century warming of a
721 large Antarctic ice-shelf cavity by a redirected coastal current. *Nature* 485, 225-228.

722 Hillenbrand, C.-D., Bentley, M.J., Stollendorf, T.D., Hein, A.S., Kuhn, G., Graham, A.G.C., Fogwill, C.J.,
723 Kristoffersen, Y., Smith, J.A., Anderson, J.B., Larter, R.D., Melles, M., Hodgson, D.A., Mulvaney, R.,
724 Sugden, D.E., 2014. Reconstruction of changes in the Weddell Sea sector of the Antarctic Ice Sheet since
725 the Last Glacial Maximum. *Quat. Sci. Rev.* 100, 111-136.

726 Hillenbrand, C.-D., Melles, M., Kuhn, G., Larter, R.D., 2012. Marine geological constraints for the grounding-
727 line position of the Antarctic Ice Sheet on the southern Weddell Sea shelf at the Last Glacial Maximum.
728 *Quat. Sci. Rev.* 32, 25-47.

729 Hodgson, D.A., Bentley, M.J., 2013. Lake highstands in the Pensacola Mountains and Shackleton Range
730 4300-2250 cal. yr BP: Evidence of a warm climate anomaly in the interior of Antarctica. *Holocene* 23,
731 388-397.

732 Joughin, I., Bamber, J.L., 2005. Thickening of the ice stream catchments feeding the Filchner-Ronne Ice
733 Shelf, Antarctica. *Geophys. Res. Lett.* 32.

734 King, M.A., Bingham, R.J., Moore, P., Whitehouse, P.L., Bentley, M.J., Milne, G.A., 2012. Lower satellite-
735 gravimetry estimates of Antarctic sea-level contribution. *Nature* 491, 586-+.

736 Kohl, C.P., Nishiizumi, K., 1992. Chemical Isolation of Quartz for Measurement of Insitu-Produced
737 Cosmogenic Nuclides. *Geochim. Cosmochim. Acta* 56, 3583-3587.

738 Lal, D., 1991. Cosmic-ray labeling of erosion surfaces - in situ nuclide production-rates and erosion models.
739 *Earth Planet. Sci. Lett.* 104, 424-439.

740 Larter, R.D., Graham, A.G.C., Hillenbrand, C.-D., Smith, J.A., Gales, J.A., 2012. Late Quaternary grounded ice
741 extent in the Filchner Trough, Weddell Sea, Antarctica: new marine geophysical evidence. *Quat. Sci. Rev.*
742 53, 111-122.

743 Le Brocq, A.M., Bentley, M.J., Hubbard, A., Fogwill, C.J., Sugden, D.E., Whitehouse, P.L., 2011.
744 Reconstructing the Last Glacial Maximum ice sheet in the Weddell Sea embayment, Antarctica, using
745 numerical modelling constrained by field evidence. *Quat. Sci. Rev.* 30, 2422-2432.

746 Lifton, N., Sato, T., Dunai, T.J., 2014. Scaling in situ cosmogenic nuclide production rates using analytical
747 approximations to atmospheric cosmic-ray fluxes. *Earth Planet. Sci. Lett.* 386, 149-160.

748 Mackintosh, A., Golledge, N., Domack, E., Dunbar, R., Leventer, A., White, D., Pollard, D., DeConto, R., Fink,
749 D., Zwartz, D., Gore, D., Lavoie, C., 2011. Retreat of the East Antarctic ice sheet during the last glacial
750 termination. *Nature Geoscience* 4, 195-202.

751 Marrero, S., Phillips, F.M., Borchers, B., Lifton, N., Aumer, R., Balco, G., 2015. Cosmogenic Nuclide
752 Systematics and the CRONUScal Program. *Quat. Geochronol.* CRONUS-Earth Special Volume.

753 Matsuoka, K., Hindmarsh, R.C.A., Moholdt, G., Bentley, M.J., Pritchard, H.D., Brown, J., Conway, H., Drews,
754 R., Durand, G., Goldberg, D., Hattermann, T., Kingslake, J., Lenaerts, J.T.M., Martín, C., Mulvaney, R.,
755 Nicholls, K.W., Pattyn, F., Ross, N., Scambos, T., Whitehouse, P.L., 2015. Antarctic ice rises and rumples:
756 Their properties and significance for ice-sheet dynamics and evolution. *Earth-Science Reviews* 150, 724-
757 745.

758 Mulvaney, R., Arrowsmith, C., Barnola, J., McCormack, T., Loulergue, L., Raynaud, D., Lipenkov, V.,
759 Hindmarsh, R., 2007. A deglaciation climate and ice sheet history of the Weddell Sea region from the
760 Berkner Island ice core. *Quat. Int.* 167-168, 294-295.

761 Nishiizumi, K., 2004. Preparation of Al-26 AMS standards. Nucl. Instrum. Methods Phys. Res. Sect. B-Beam
762 Interact. Mater. Atoms 223-24, 388-392.

763 Nishiizumi, K., Imamura, M., Caffee, M.W., Southon, J.R., Finkel, R.C., McAninch, J., 2007. Absolute
764 calibration of Be-10 AMS standards. Nucl. Instrum. Methods Phys. Res. Sect. B-Beam Interact. Mater.
765 Atoms 258, 403-413.

766 Ross, N., Bingham, R.G., Corr, H.F.J., Ferraccioli, F., Jordan, T.A., Le Brocq, A., Rippin, D.M., Young, D.,
767 Blankenship, D.D., Siegert, M.J., 2012. Steep reverse bed slope at the grounding line of the Weddell Sea
768 sector in West Antarctica. Nature Geoscience 5, 393-396.

769 Schmidt, D.L., Williams, P.L., Nelson, W.H., 1978. Geologic map of the Schmidt Hills Quadrangle and part of
770 the Gambacorta Peak Quadrangle, Pensacola Mountains, Antarctica, Antarctic Map, - ed, Reston, VA.

771 Schoof, C., 2007. Ice sheet grounding line dynamics: Steady states, stability, and hysteresis. J. Geophys.
772 Res.-Earth Surf. 112.

773 Shepherd, A., Ivins, E.R., Geruo, A., Barletta, V.R., Bentley, M.J., Bettadpur, S., Briggs, K.H., Bromwich, D.H.,
774 Forsberg, R., Galin, N., Horwath, M., Jacobs, S., Joughin, I., King, M.A., Lenaerts, J.T.M., Li, J.L.,
775 Ligtenberg, S.R.M., Luckman, A., Luthcke, S.B., McMillan, M., Meister, R., Milne, G., Mouginot, J., Muir,
776 A., Nicolas, J.P., Paden, J., Payne, A.J., Pritchard, H., Rignot, E., Rott, H., Sorensen, L.S., Scambos, T.A.,
777 Scheuchl, B., Schrama, E.J.O., Smith, B., Sundal, A.V., van Angelen, J.H., van de Berg, W.J., van den
778 Broeke, M.R., Vaughan, D.G., Velicogna, I., Wahr, J., Whitehouse, P.L., Wingham, D.J., Yi, D.H., Young, D.,
779 Zwally, H.J., 2012. A Reconciled Estimate of Ice-Sheet Mass Balance. Science 338, 1183-1189.

780 Siegert, M., Ross, N., Corr, H., Kingslake, J., Hindmarsh, R., 2013. Late Holocene ice-flow reconfiguration in
781 the Weddell Sea sector of West Antarctica. Quat. Sci. Rev. 78, 98-107.

782 Stone, J.O., 2000. Air pressure and cosmogenic isotope production. J. Geophys. Res.-Solid Earth 105, 23753-
783 23759.

784 Suganuma, Y., Miura, H., Zondervan, A., Okuno, J., 2014. East Antarctic deglaciation and the link to global
785 cooling during the Quaternary: evidence from glacial geomorphology and Be-10 surface exposure dating
786 of the Sor Rondane Mountains, Dronning Maud Land. Quat. Sci. Rev. 97, 102-120.

787 Sugden, D.E., Balco, G., Cowdery, S.G., Stone, J.O., Sass, L.C., 2005. Selective glacial erosion and weathering
788 zones in the coastal mountains of Marie Byrd Land, Antarctica. Geomorphology 67, 317-334.

789 Velicogna, I., Sutterley, T.C., van den Broeke, M.R., 2014. Regional acceleration in ice mass loss from
790 Greenland and Antarctica using GRACE time-variable gravity data. Geophys. Res. Lett. 41, 8130-8137.

791 White, D., Fueloep, R.-H., Bishop, P., Mackintosh, A., Cook, G., 2011. Can in-situ cosmogenic (14)C be used
792 to assess the influence of clast recycling on exposure dating of ice retreat in Antarctica? Quat.
793 Geochronol. 6, 289-294.

794 Whitehouse, P.L., Bentley, M.J., Le Brocq, A.M., 2012. A deglacial model for Antarctica: geological
795 constraints and glaciological modelling as a basis for a new model of Antarctic glacial isostatic
796 adjustment. Quat. Sci. Rev. 32, 1-24.

797 Whitehouse, P.L., Bentley, M.J., Vieli, A., Jamieson, S.S.R., Hein, A.S., Sugden, D.E., submitted. Controls on
798 Last Glacial Maximum ice expansion in the Weddell Sea embayment, Antarctica. J. Geophys. Res.-Earth
799 Surf.

800 Williams, S.D.P., Moore, P., King, M.A., Whitehouse, P.L., 2014. Revisiting GRACE Antarctic ice mass trends
801 and accelerations considering autocorrelation. Earth Planet. Sci. Lett. 385, 12-21.

802 Wright, A.P., Le Brocq, A.M., Cornford, S.L., Bingham, R.G., Corr, H.F.J., Ferraccioli, F., Jordan, T.A., Payne,
803 A.J., Rippin, D.M., Ross, N., Siegert, M.J., 2014. Sensitivity of the Weddell Sea sector ice streams to sub-
804 shelf melting and surface accumulation. The Cryosphere 8, 2119-2134.

805 Xu, S., Dougans, A.B., Freeman, S., Schnabel, C., Wilcken, K.M., 2010. Improved Be-10 and Al-26-AMS with a
806 5 MV spectrometer. Nucl. Instrum. Methods Phys. Res. Sect. B-Beam Interact. Mater. Atoms 268, 736-
807 738.

808 Xu, S., Freeman, S.P.H.T., Rood, D.H., Shanks, R.P., 2014. Al-26 interferences in accelerator mass
809 spectrometry measurements. Nucl. Instrum. Methods Phys. Res. Sect. B-Beam Interact. Mater. Atoms
810 333, 42-45.

811 Xu, S., Freeman, S.P.H.T., Sanderson, D., Shanks, R.P., Wilcken, K.M., 2013. Cl can interfere with Al3+ AMS
812 but B need not matter to Be measurement. Nucl. Instrum. Methods Phys. Res. Sect. B-Beam Interact.
813 Mater. Atoms 294, 403-405.

Table 1 revised

Table 1 Rock sample details and cosmogenic ^{10}Be and ^{26}Al concentrations in quartz-bearing erratics.															
Location	Sample ID	Lat.	Long.	Alt.	Lithology	Thickness	Topo shielding	Quartz mass	^{10}Be AMS ID [†]	^{10}Be concn [§]	$\pm 1\sigma$ ^{10}Be	^{26}Al AMS ID [†]	^{26}Al concn [#]	$\pm 1\sigma$ ^{26}Al	
		(dd)	(dd)	(m asl)		(cm)		(g)		(atom g ⁻¹ [SiO ₂])	(atom g ⁻¹ [SiO ₂])		(atom g ⁻¹ [SiO ₂])	(atom g ⁻¹ [SiO ₂])	
Pillow Knob	WIL-1	-83.65392	-58.63597	689	Qtz ss	3.0	0.999	30.933	b4558	6.536E+04	3.219E+03				
Pillow Knob	WIL-3	-83.65240	-58.63180	722	P congl.	3.5	0.997	29.819	b4559	6.007E+04	2.679E+03				
Pillow Knob	WIL-4	-83.65185	-58.63303	743	Qtz ss	4.0	0.998	26.054	b7805	5.180E+04	4.176E+03				
Pillow Knob	WIL-5	-83.65182	-58.63197	746	Qtz ss	4.0	0.998	28.863	b5258	8.226E+04	2.785E+03	a2004	5.228E+05	3.620E+04	
Pillow Knob	WIL-6	-83.65067	-58.62528	780	P congl.	4.0	1.000	28.513	b7806	7.512E+04	5.347E+03				
Teeny Rock	WIL-8	-83.64213	-58.95122	572	Qtz ss	4.5	0.999	29.004	b4564	5.440E+04	2.792E+03				
Teeny Rock	WIL-13	-83.63807	-58.99585	529	Qtz ss	3.5	1.000	32.214	b5259	4.762E+04	2.038E+03	a2005	3.178E+05	2.389E+04	
Teeny Rock	WIL-15	-83.63615	-59.00812	500	Qtz ss	3.5	1.000	31.494	b4565	5.794E+04	3.458E+03				
Teeny Rock	WIL-16	-83.62843	-59.10403	459	Qtz ss	4.5	1.000	26.893	b5260	2.604E+06	7.854E+04				
Teeny Rock	WIL-17	-83.62835	-59.10415	442	Qtz ss	3.0	1.000	26.474	b4566	4.085E+04	2.701E+03				
Storey Peak	WIL-18	-83.67310	-58.64347	861	Qtz ss banded	4.0	1.000	27.880	b5261	1.214E+05	4.375E+03				
Storey Peak	WIL-19	-83.67243	-58.66825	841	Qtz phenocryst	6.0	1.000	24.468	b7807	7.137E+04	4.185E+03				
Storey Peak	WIL-20	-83.67233	-58.67065	838	Qtz ss	5.0	1.000	27.784	b5262	9.142E+04	3.785E+03				
Storey Peak	WIL-21	-83.67223	-58.67187	831	SS impure	8.0	1.000	28.355	b4568	1.059E+05	4.977E+03				
Mt Hobbs	WIL-26	-83.74648	-58.80223	1055	Qtz ss	4.0	1.000	25.519	b4569	1.217E+05	5.115E+03				
Mt Hobbs	WIL-27	-83.74212	-58.80662	1055	Qtz microcrystalline	3.0	1.000	4.565	b5264	6.866E+06	2.131E+05				
McConnachie Rock	WIL-28	-83.74122	-59.07610	621	Qtz ss	3.5	0.998	28.801	b4570	5.396E+04	3.079E+03				
McConnachie Rock	WIL-31	-83.74275	-59.08593	665	Qtz ss fine/grey	3.5	0.999	26.641	b7809	1.043E+06	2.879E+04				
McConnachie Rock	WIL-32	-83.74827	-59.04553	796	Qtz ss	3.5	1.000	28.008	b4574	8.821E+04	3.818E+03				
McConnachie Rock	WIL-33	-83.74803	-59.04458	795	Qtz ss	5.0	1.000	29.350	b7810	7.489E+04	3.831E+03				
Mt Bragg	BRG-1	-84.09852	-56.78165	1048	Qtz ss	3.0	0.999	26.368	b4575	2.686E+05	7.721E+03				
Mt Bragg	BRG-2	-84.09852	-56.78250	1047	Qtz ss	6.0	0.999	27.818	b7816	1.862E+05	5.954E+03				
Mt Bragg	BRG-4	-84.09835	-56.78345	1049	Qtz ss banded	3.5	0.999	32.423	b7817	1.087E+05	3.788E+03				
Mt Bragg	BRG-5	-84.09655	-56.80657	1002	Qtz ss pebble	3.5	0.997	28.681	b4576	2.559E+06	5.768E+04				

Mt Bragg	BRG-6	-84.09652	-56.80710	1000	Qtzite banded	4.0	0.997	25.686	b5266	5.306E+05	1.677E+04			
Mt Bragg	BRG-7	-84.09652	-56.80768	1000	Qtz ss	3.0	0.997	29.849	b5267	9.543E+05	3.007E+04			
Mt Bragg	BRG-8	-84.09650	-56.80785	1000	Qtz ss	5.5	0.997	27.404	b4577	4.660E+05	1.236E+04			
Mt Bragg	BRG-9	-84.09373	-56.83290	898	Qtz ss	3.5	0.990	29.200	b7818	1.661E+06	4.394E+04			
Mt Bragg	BRG-10	-84.09368	-56.82920	900	Qtz ss	6.0	0.990	26.916	b7819	1.775E+06	4.009E+04			
Mt Bragg	BRG-11	-84.09430	-56.85667	814	Qtz ss Qtz ss red/banded	5.0	0.994	26.708	b4579	1.497E+06	3.346E+04			
Mt Bragg	BRG-13	-84.09142	-56.78210	1196	Qtz ss	5.0	1.000	25.928	b4580	4.977E+06	1.091E+05			
Mt Bragg	BRG-14	-84.09138	-56.78278	1196	Qtz ss	4.0	1.000	29.499	b7820	2.730E+05	8.882E+03			
Mt Bragg	BRG-15	-84.09433	-56.77607	1125	Qtz ss	4.0	0.999	30.048	b4581	2.057E+06	4.622E+04			
Mt Bragg	BRG-16	-84.09433	-56.77607	1125	Qtz ss	3.0	0.999	28.414	b7822	5.259E+06	1.096E+05			
Mt Bragg	BRG-19	-84.09908	-56.77937	1030	Qtz ss	3.0	0.996	30.337	b4590	2.078E+06	4.578E+04			
Mt Bragg	BRG-20	-84.09907	-56.78190	1030	Qtz ss	3.0	0.996	28.145	b5270	1.591E+05	5.159E+03	a2007	1.113E+06	6.579E+04
Mt Bragg	BRG-21	-84.10288	-56.78340	920	Qtz ss	5.5	0.994	26.161	b4591	1.712E+06	3.831E+04			
Mt Bragg	BRG-22	-84.10285	-56.78333	920	Qtz ss	6.0	0.994	26.563	b5271	1.568E+06	4.741E+04			
Mt Bragg	BRG-23	-84.10428	-56.77825	870	Qtz ss	3.0	0.994	27.583	b4592	3.105E+06	6.851E+04			
Mt Bragg	BRG-24	-84.10417	-56.77890	872	Qtz ss	7.0	0.994	25.963	b5272	1.255E+06	3.874E+04			
Mt Bragg	BRG-25	-84.10485	-56.78243	842	Qtz ss grey	3.5	0.992	26.301	b4593	2.245E+06	4.949E+04			
Mt Bragg	BRG-26	-84.10495	-56.78202	840	Qtz ss	3.5	0.992	32.044	b5273	4.620E+04	2.148E+03	a2008	3.076E+05	2.604E+04
Mt Bragg	BRG-27	-84.10540	-56.78197	816	Qtz ss	5.0	0.898	29.210	b4595	2.536E+04	1.788E+03			
Mt Bragg	BRG-28	-84.10537	-56.78232	813	Qtz ss	3.5	0.898	32.358	b5274	2.338E+05	7.478E+03			
Mt Harper	HAR-1	-84.07052	-57.11272	878	Qtz ss	3.5	1.000	29.411	b5277	5.215E+04	2.193E+03	a2011	3.943E+05	2.978E+04
Mt Harper	HAR-2	-84.07055	-57.11340	878	Qtz ss	4.5	1.000	31.937	b5278	4.940E+04	1.988E+03			
Mt Harper	HAR-3	-84.07080	-57.11153	878	Qtz ss	4.0	1.000	28.348	b7811	3.738E+04	3.079E+03			
Mt Harper	HAR-4	-84.06193	-57.12530	913	Qtz ss	4.0	1.000	24.055	b4827	7.461E+04	3.089E+03			
Mt Harper	HAR-5	-84.06193	-57.12530	913	Qtz ss	4.0	1.000	27.739	b5279	6.918E+04	2.568E+03	a2012	5.346E+05	3.718E+04
Mt Harper	HAR-6	-84.06105	-57.19130	840	Qtz ss	3.5	1.000	31.845	b4596	7.855E+04	3.565E+03			
Mt Harper	HAR-7	-84.06100	-57.19182	840	Qtz ss	3.5	1.000	28.209	b5282	8.732E+04	3.181E+03	a2013	6.521E+05	4.638E+04
Mt Harper	HAR-8	-84.05772	-57.19725	782	Qtz ss	6.0	0.999	28.401	b5283	5.514E+04	2.260E+03			
Mt Harper	HAR-9	-84.05772	-57.19725	780	Qtz ss banded	4.5	0.999	28.276	b5284	3.608E+05	1.151E+04			
Mt Harper	HAR-10	-84.05935	-57.24463	734	Qtz ss	2.5	0.999	29.241	b4597	1.544E+05	5.735E+03			

Mt Harper	HAR-11	-84.05935	-57.24463	734	Qtz ss	7.0	0.999	30.887	b5285	9.731E+04	3.614E+03			
Dimmo Peak	SCH-7	-83.32930	-58.01092	560	Qtz ss	6.0	0.993	25.140	b5246	1.891E+06	5.726E+04			
Mt Nervo	SCH-10	-83.23432	-57.99215	874	Qtz ss	2.5	1.000	27.294	b5247	1.292E+07	2.851E+05			
Mt Nervo	SCH-11	-83.23410	-57.99407	876	Qtz pegmatite	5.5	1.000	26.899	b5248	1.796E+07	3.809E+05			
Mt Nervo	SCH-13	-83.23402	-58.00913	829	Qtz ss	3.5	0.998	30.311	b5249	6.426E+06	1.422E+05			
Mt Nervo	SCH-19	-83.23785	-58.13295	400	Qtz ss	3.5	0.999	30.525	b5250	2.139E+06	6.429E+04			
Mt Nervo	SCH-20	-83.23780	-58.13248	401	Qtz ss banded	5.0	0.999	26.490	b5252	1.993E+06	5.724E+04			
Gordon Spur	SCH-21	-83.27373	-58.13032	667	Qtz	5.0	1.000	29.030	b5253	1.032E+07	2.269E+05			
Gordon Spur	SCH-25	-83.27035	-58.10953	728	Qtz ss banded	5.0	1.000	28.297	b5255	8.647E+06	1.907E+05			
Clapperton Ridge	THO-1	-84.34060	-65.04507	730	Qtz ss banded	5.0	1.000	31.741	b4804	7.129E+06	1.594E+05			
Clapperton Ridge	THO-3	-84.34245	-65.01345	782	Qtz ss	4.5	0.998	26.591	b4807	7.128E+06	1.534E+05	a1406	3.382E+07	1.742E+06
Clapperton Ridge	THO-5	-84.34458	-65.00268	840	Qtz	5.0	0.998	30.046	b4808	8.510E+06	1.899E+05	a1409	3.983E+07	2.037E+06
Sugden Ridge	THO-7	-84.34243	-65.19182	465	Qtz ss fine	5.0	0.986	27.083	b4809	3.120E+05	1.013E+04			
Sugden Ridge	THO-8	-84.34248	-65.19147	465	Qtz ss	4.0	0.986	30.234	b4810	1.947E+05	6.561E+03			
Sugden Ridge	THO-9	-84.34248	-65.19147	465	Qtzite	4.0	0.986	26.553	b6690	2.263E+05	7.773E+03	a2017	1.570E+06	9.190E+04
Sugden Ridge	THO-10	-84.34248	-65.19147	465	Qtz ss grey	6.0	0.986	27.895	b6691	2.208E+05	8.796E+03	a2018	1.371E+06	8.391E+04
Sugden Ridge	THO-11	-84.34565	-65.18108	520	P. congl.	5.0	0.988	25.974	b4811	4.131E+05	1.212E+04			
Sugden Ridge	THO-12	-84.34560	-65.18220	530	Qtz ss fine	3.0	0.988	32.211	b4813	2.732E+05	7.576E+03			
Sugden Ridge	THO-13	-84.34315	-65.16932	414	Qtz ss	4.5	0.993	26.538	b4815	2.633E+05	8.573E+03			
Sugden Ridge	THO-14	-84.34313	-65.16890	414	Qtz ss	3.0	0.993	28.066	b4816	2.110E+05	6.868E+03			
Sugden Ridge	THO-15	-84.34310	-65.16948	414	Qtz ss grey	3.5	0.993	25.286	b6693	9.605E+04	4.508E+03	a2019	6.546E+05	4.278E+04
Sugden Ridge	THO-16	-84.34312	-65.16980	414	Qtz ss fine	3.0	0.993	25.511	b6694	1.744E+05	6.502E+03	a2020	1.133E+06	6.609E+04
Sugden Ridge	THO-17	-84.34065	-65.18838	410	Qtz ss	4.0	0.992	27.548	b4819	3.376E+05	1.055E+04			
Sugden Ridge	THO-18	-84.34063	-65.18847	410	Qtz ss	3.0	0.992	26.848	b4820	2.152E+05	6.114E+03			
Sugden Ridge	THO-19	-84.34055	-65.18920	410	Qtz ss	4.0	0.992	26.434	b6695	2.587E+06	6.105E+04			
Sugden Ridge	THO-20	-84.34055	-65.18918	410	Qtz ss	4.0	0.992	29.049	b6696	2.147E+06	5.123E+04			
Sugden Ridge	THO-21	-84.34915	-65.14835	545	Qtz	4.0	0.998	29.180	b4821	4.187E+06	9.144E+04	a1411	2.318E+07	1.213E+06
Sugden Ridge	THO-24	-84.34355	-65.22095	635	Qtz ss	5.0	0.999	30.388	b4822	8.690E+05	2.201E+04	a1412	5.858E+06	3.152E+05
Sugden Ridge	THO-25	-84.34150	-65.20867	480	Qtz ss	3.5	0.970	28.501	b6697	1.309E+06	3.463E+04			
Sugden Ridge	THO-26	-84.34152	-65.20773	477	Qtzite green	3.5	0.970	26.327	b6702	1.405E+06	3.799E+04			

Sugden Ridge	THO-27	-84.34155	-65.20773	477	Qtz ss pebbles	5.0	0.984	29.669	b4823	2.313E+05	7.590E+03			
Sugden Ridge	THO-28	-84.34155	-65.20689	475	Qtz ss pebbles	4.0	0.984	25.036	b4826	2.650E+05	9.416E+03			
Bentley Peak	THN-7	-84.29638	-64.23857	570	Qtz ss	3.5	0.998	29.953	b6709	4.196E+06	9.372E+04			
Bentley Peak	THN-8	-84.29648	-64.23945	570	Qtz pegmatite	3.0	0.998	30.031	b6711	4.586E+06	1.033E+05			
Bentley Peak	THN-10	-84.29493	-64.26187	515	Qtz ss fine	4.0	0.999	29.965	b6715	3.801E+04	5.815E+03	a2023	3.337E+05	2.404E+04
Bentley Peak	THN-12	-84.28612	-64.31283	390	Qtz ss coarse	3.5	0.998	27.224	b6716	3.751E+05	1.453E+04			
Bentley Peak	THN-13	-84.28595	-64.31307	390	Qtz ss fine	3.5	0.998	25.248	b6717	5.929E+05	2.558E+04			
Bentley Peak	THN-15	-84.28683	-64.32338	435	Qtz ss	4.0	0.998	28.907	b6718	5.490E+05	2.015E+04			
Bentley Peak	THN-17	-84.28683	-64.33273	463	Qtzite	3.5	0.997	27.667	b6719	3.588E+05	1.398E+04			
Mt Yarborough	YAR-1	-84.41220	-65.93483	848	Qtz ss fine	4.5	0.999	26.235	b4837	7.647E+06	1.668E+05	a1421	3.711E+07	1.887E+06
Mt Yarborough	YAR-2	-84.41225	-65.93440	850	Qtz ss	5.5	0.999	27.533	b4838	8.145E+06	1.820E+05			
Mt Yarborough	YAR-5	-84.41005	-65.99980	790	Qtz ss fine	6.0	1.000	32.110	b4839	5.143E+06	1.126E+05	a1422	2.975E+07	1.516E+06
Mt Yarborough	YAR-7	-84.40942	-66.01725	768	Qtz ss	4.0	0.999	29.899	b4840	6.424E+06	1.437E+05			
Mt Yarborough	YAR-9	-84.40735	-66.02582	710	Qtz ss	6.0	0.999	31.709	b4843	3.286E+06	7.102E+04			
Mt Yarborough	YAR-11	-84.40703	-66.01277	690	Qtz ss	4.5	0.998	24.883	b4844	2.341E+06	5.337E+04			
Mt Yarborough	YAR-12	-84.40700	-66.01237	690	Qtz ss	5.0	0.998	26.325	b6703	3.266E+06	7.319E+04			
Mt Yarborough	YAR-14	-84.40555	-65.99897	670	Qtz ss	3.0	0.998	31.048	b6704	5.258E+06	1.139E+05			
Mt Yarborough	YAR-15	-84.40395	-65.97610	642	Qtz ss pink	5.0	0.998	29.025	b6705	3.038E+06	6.669E+04			
Mt Yarborough	YAR-16	-84.40403	-65.97715	644	Qtz ss	4.0	0.998	26.872	b4845	4.426E+06	9.967E+04			
Mt Yarborough	YAR-17	-84.40345	-65.96642	615	Qtz pegmatite	7.0	0.993	30.595	b6707	4.396E+06	9.391E+04			
Mt Yarborough	YAR-18	-84.40342	-65.96640	615	Qtz ss	4.0	0.993	29.136	b6708	5.360E+06	1.143E+05			

*SS: sandstone; Qtz: quartz; Qtzite: quartzite; P. cong.: pebble conglomerate. Assumed R_ρ rock density 2.7 g cm⁻³.

[†]AMS measurements made at Scottish Universities Environmental Research Centre (SUERC).

[§]Normalised to NIST SRM-4325 Be standard material with a revised nominal ¹⁰Be/⁹Be ratio (2.79 x 10⁻¹¹) (Nishiizumi et al., 2007) ~~and half-life of 1.387 Ma (Chmeleff et al., 2010; Korschinek et al., 2010)~~ and corrected for process blanks; uncertainties include propagated AMS sample/lab-blank uncertainty and a 2% carrier mass uncertainty.

[#]Normalised to the Purdue Z92-0222 Al standard material with a nominal ²⁷Al/²⁶Al ratio of 4.11 x 10⁻¹¹ that agrees with Al standard material of Nishiizumi et al. (2004), and corrected for process blanks; uncertainties include propagated AMS sample/lab-blank uncertainty and a 5% stable ²⁷Al measurement (ICP-OES) uncertainty.

Table 2. Cosmogenic ^{10}Be and ^{26}Al surface exposure ages.

Sample ID	Alt.	^{10}Be age* \pm 1σ (int) [†]	$\pm 1\sigma$ (ext) [†] ^{10}Be	$\pm 1\sigma$ (full) [†] ^{10}Be	^{26}Al age* \pm 1σ (int) [†]	$\pm 1\sigma$ (ext) [†] ^{26}Al	$\pm 1\sigma$ (full) [†] ^{26}Al	$^{26}\text{Al}/^{10}\text{Be}$ \pm 1σ	Regional ice surface [^]	Height above present ice [^]
	(m)	(ka)	(ka)	(ka)	(ka)	(ka)	(ka)		(m)	(m)
WIL-1	689	6.60 \pm 0.29	0.64	0.83					550	139
WIL-3	722	5.91 \pm 0.27	0.51	0.70					550	172
WIL-4	743	5.00 \pm 0.46	0.60	0.73					550	193
WIL-5	746	7.87 \pm 0.26	0.63	0.90	6.98 \pm 0.47	0.89	1.0	6.36 \pm 0.49	550	196
WIL-6	780	7.00 \pm 0.47	0.72	0.89					550	230
WIL-8	572	6.21 \pm 0.31	0.55	0.75					400	172
WIL-13	529	5.60 \pm 0.22	0.49	0.66	5.17 \pm 0.39	0.72	0.83	6.67 \pm 0.58	400	129
WIL-15	500	7.02 \pm 0.45	0.69	0.87					400	100
WIL-16	459	362 \pm 12	33	46					400	59
WIL-17	442	5.22 \pm 0.33	0.52	0.66					400	42
WIL-18	861	10.5 \pm 0.4	0.9	1.3					575	286
WIL-19	841	6.41 \pm 0.38	0.61	0.80					575	266
WIL-20	838	8.14 \pm 0.31	0.73	0.99					575	263
WIL-21	831	9.70 \pm 0.48	0.93	1.2					575	256
WIL-26	1055	8.85 \pm 0.39	0.84	1.1					600	455
WIL-27	1055	572 \pm 21	55	77					600	455
WIL-28	621	5.83 \pm 0.35	0.57	0.74					500	121
WIL-31	665	111 \pm 3	9	13					500	165
WIL-32	796	8.06 \pm 0.36	0.69	0.96					500	296
WIL-33	795	6.99 \pm 0.33	0.66	0.85					500	295
BRG-1	1048	19.7 \pm 0.6	1.6	2.3					810	238
BRG-2	1047	14.0 \pm 0.4	1.2	1.6					810	237
BRG-4	1049	7.86 \pm 0.28	0.63	0.89					810	239
BRG-5	1002	206 \pm 5	17	25					810	192
BRG-6	1000	41.1 \pm 1.3	3.5	4.9					810	190
BRG-7	1000	74.0 \pm 2.4	6.3	8.8					810	190
BRG-8	1000	37.0 \pm 1.0	3.0	4.2					810	190
BRG-9	898	146 \pm 4	12	17					810	88
BRG-10	900	158 \pm 4	13	19					810	90
BRG-11	814	142 \pm 3	12	17					810	4
BRG-13	1196	353 \pm 8	31	44					813	383
BRG-14	1196	17.6 \pm 0.6	1.5	2.1					813	383
BRG-15	1125	147 \pm 3	12	17					813	312

BRG-16	1125	395 ± 9	35	50					813	312
BRG-19	1030	161 ± 4	14	19					813	217
BRG-20	1030	12.0 ± 0.4	1.0	1.4	11.5 ± 0.7	1.4	1.7	7.00 ± 0.47	813	217
BRG-21	920	149 ± 3	12	18					813	107
BRG-22	920	136 ± 4	12	16					813	107
BRG-23	870	286 ± 7	25	35					813	57
BRG-24	872	115 ± 4	10	14					813	59
BRG-25	842	209 ± 5	18	25					813	29
BRG-26	840	4.07 ± 0.19	0.39	0.53	3.73 ± 0.35	0.51	0.60	6.66 ± 0.64	813	27
BRG-27	816	2.51 ± 0.22	0.28	0.35					813	3
BRG-28	813	24.0 ± 0.7	2.0	2.8					813	0
HAR-1	878	4.44 ± 0.20	0.38	0.53	4.65 ± 0.39	0.64	0.75	7.56 ± 0.65	710	168
HAR-2	878	4.23 ± 0.18	0.36	0.51					710	168
HAR-3	878	3.14 ± 0.26	0.38	0.46					710	168
HAR-4	913	6.20 ± 0.23	0.56	0.74					710	203
HAR-5	913	5.70 ± 0.23	0.50	0.68	6.15 ± 0.40	0.71	0.87	7.73 ± 0.61	710	203
HAR-6	840	6.90 ± 0.30	0.62	0.82					710	130
HAR-7	840	7.62 ± 0.28	0.62	0.87	8.00 ± 0.50	1.0	1.2	7.47 ± 0.60	710	130
HAR-8	782	5.25 ± 0.21	0.43	0.59					710	72
HAR-9	780	34.0 ± 1.1	2.9	4.0					710	70
HAR-10	734	14.9 ± 0.6	1.3	1.8					710	24
HAR-11	734	9.71 ± 0.39	0.89	1.2					710	24
SCH-7	560	236 ± 8	21	29					300	260
SCH-10	874	1570 ± 53	190	280					300	574
SCH-11	876	3000 ± 151	550	860					300	576
SCH-13	829	677 ± 18	65	93					300	529
SCH-19	400	307 ± 10	28	39					300	100
SCH-20	401	289 ± 9	26	36					300	101
SCH-21	667	1560 ± 52	190	280					300	367
SCH-25	728	1120 ± 33	120	170					300	428
THO-1	730	865 ± 24	87	130					380	350
THO-3	782	813 ± 22	81	120	573 ± 40	91	110	4.74 ± 0.26	380	402
THO-5	840	953 ± 27	98	140	670 ± 49	110	140	4.68 ± 0.26	380	460
THO-7	465	40.4 ± 1.3	3.4	4.8					380	85
THO-8	465	24.9 ± 0.8	2.1	3.0					380	85
THO-9	465	29.0 ± 1.0	2.4	3.4	27.9 ± 1.6	3.4	4.1	6.94 ± 0.47	380	85
THO-10	465	28.8 ± 1.2	2.5	3.4	25.0 ± 1.5	3.0	3.7	6.21 ± 0.45	380	85
THO-11	520	51.1 ± 1.5	4.3	6.0					380	140
THO-12	530	32.5 ± 0.9	2.7	3.8					380	150
THO-13	414	36.0 ± 1.2	3.0	4.2					380	34

THO-14	414	28.1 ± 0.9	2.4	3.3					380	34
THO-15	414	12.8 ± 0.6	1.2	1.6	12.0 ± 0.8	1.5	1.8	6.82 ± 0.55	380	34
THO-16	414	23.0 ± 0.9	2.0	2.8	20.8 ± 1.2	2.6	3.1	6.50 ± 0.45	380	34
THO-17	410	45.6 ± 1.4	3.9	5.4					380	30
THO-18	410	28.7 ± 0.8	2.4	3.3					380	30
THO-19	410	380 ± 10	34	48					380	30
THO-20	410	310 ± 8	27	39					380	30
THO-21	545	563 ± 14	52	75	470 ± 31	70	85	5.54 ± 0.31	380	165
THO-24	635	96.0 ± 2.5	8.0	11	92.0 ± 5.1	11	14	6.74 ± 0.40	380	255
THO-25	480	173 ± 5	15	21					380	100
THO-26	477	188 ± 5	16	23					380	97
THO-27	477	29.7 ± 1.0	2.5	3.5					380	97
THO-28	475	33.8 ± 1.2	2.9	4.0					380	95
THN-7	570	546 ± 14	51	72					390	180
THN-8	570	603 ± 16	57	81					390	180
THN-10	515	4.56 ± 0.75	0.84	0.92	5.54 ± 0.40	0.68	0.81	8.78 ± 1.48	390	125
THN-12	390	51.4 ± 2.0	4.5	6.2					390	0
THN-13	390	81.9 ± 3.6	7.4	10					390	0
THN-15	435	72.5 ± 2.7	6.4	8.8					390	45
THN-17	463	46.0 ± 1.8	4.0	5.5					390	73
YAR-1	848	828 ± 22	82	120	603 ± 42	97	120	4.85 ± 0.27	560	288
YAR-2	850	897 ± 25	91	130					560	290
YAR-5	790	554 ± 14	51	73	487 ± 32	73	90	5.79 ± 0.32	560	230
YAR-7	768	730 ± 20	70	100					560	208
YAR-9	710	366 ± 9	32	46					560	150
YAR-11	690	255 ± 6	22	31					560	130
YAR-12	690	367 ± 9	32	46					560	130
YAR-14	670	630 ± 16	60	86					560	110
YAR-15	642	357 ± 9	31	45					610	32
YAR-16	644	540 ± 14	50	71					610	34
YAR-17	615	569 ± 14	53	76					610	5
YAR-18	615	696 ± 18	67	96					610	5

*Ages calculated with CRONUS-Earth CRONUScalc v.2.0 (Marrero et al., 2015), LSD scaling (Lifton et al., 2014), no erosion correction; attenuation length 153 ± 10 g cm⁻², ²⁶Al and ¹⁰Be production rates from CRONUS-Earth Project (Borchers et al., 2015).

†(int) = Internal uncertainties; includes only concentration uncertainties based on lab/AMS measurements.

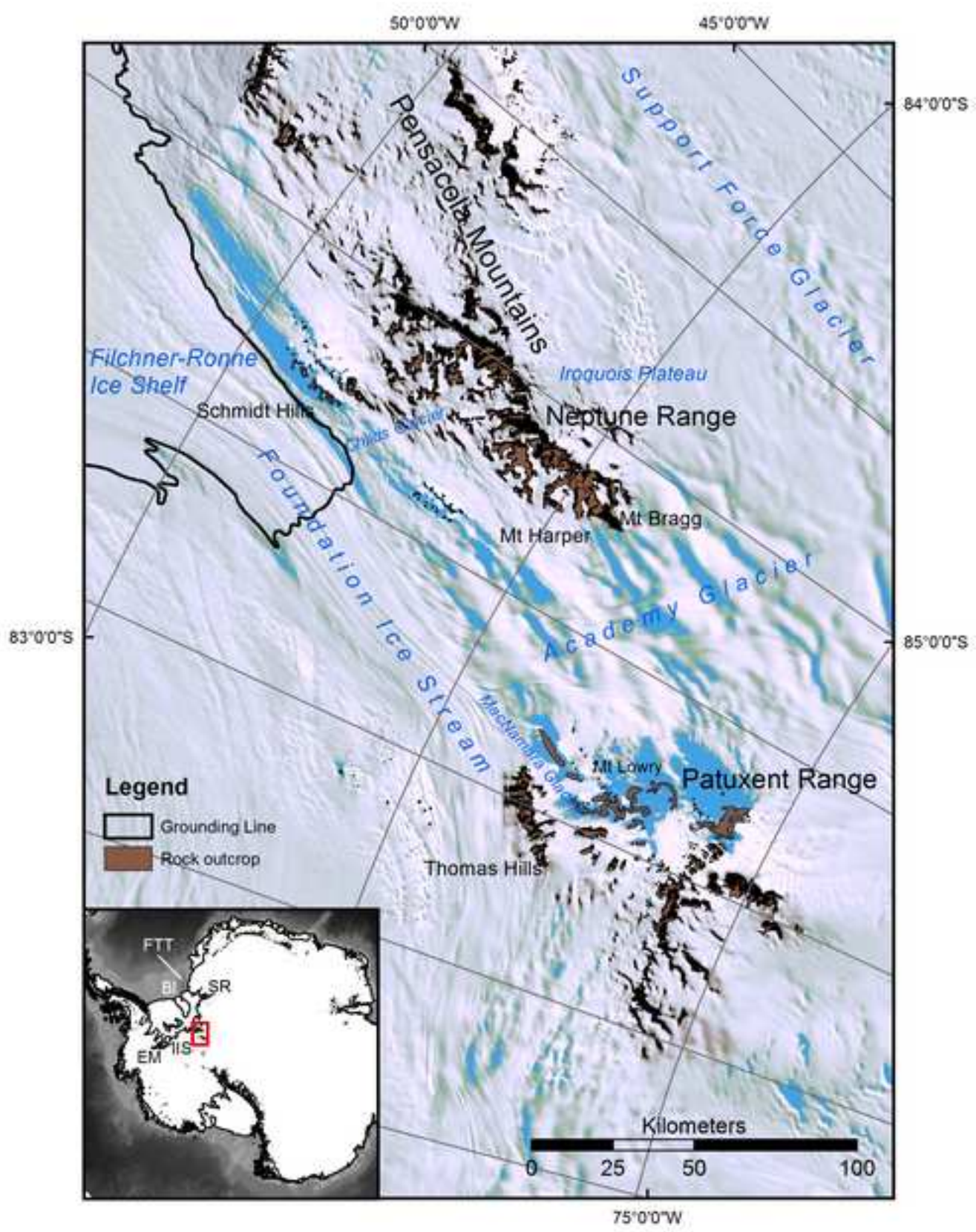
†(ext) = External uncertainties; includes internal uncertainties plus scaling and production rate uncertainties.

†(full) = Full uncertainties; includes external uncertainties plus uncertainties on thickness (0.5 cm), pressure (10 hPa), attenuation length (10 g cm⁻²), and density (0.05 g cm⁻³).

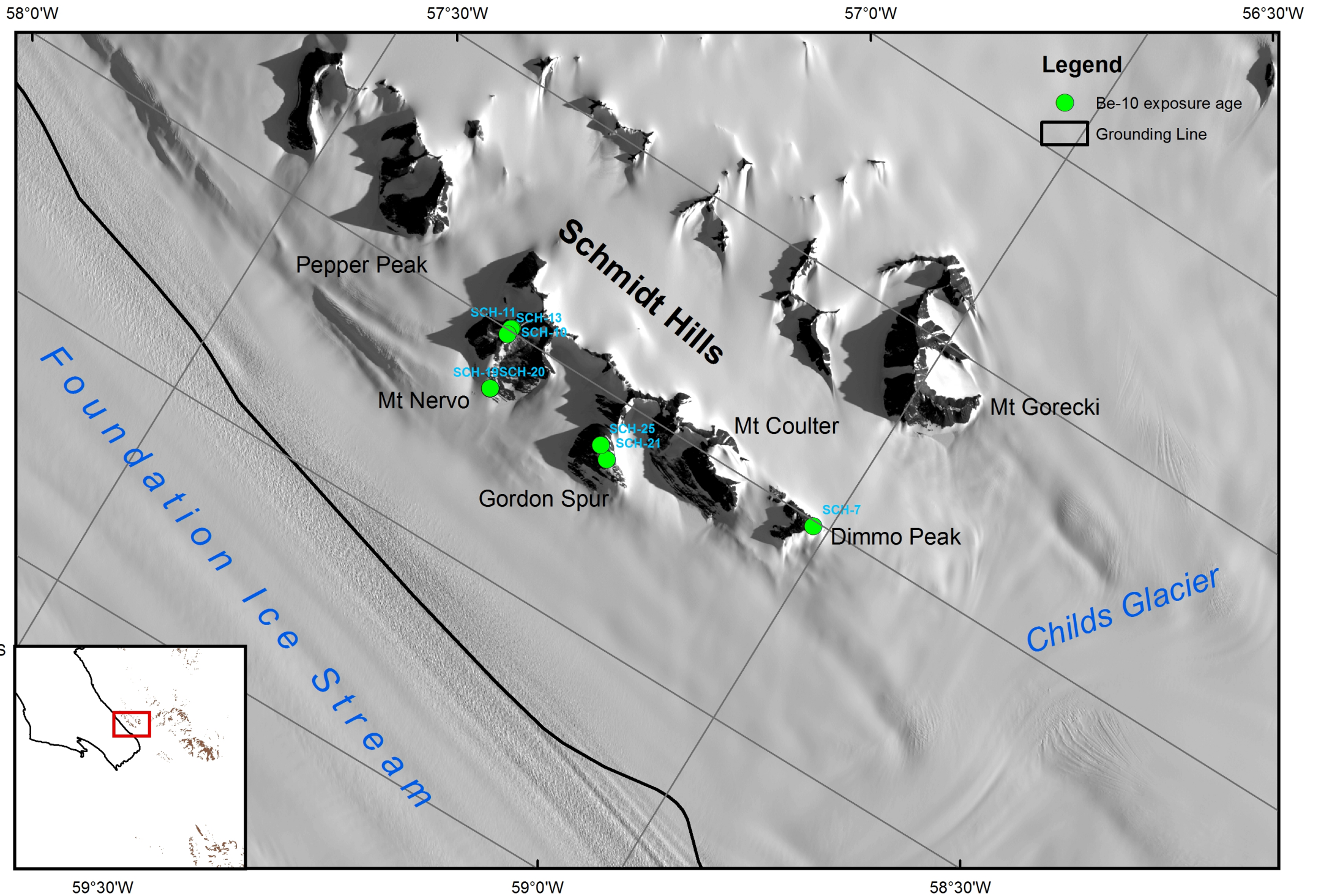
^Sample elevations are normalised to the elevation of the ice surface at the foot of the spur or peak on which the sample lies, and so the plots in Figure 4 are in terms of elevation above present ice.

Figure 1 revised

[Click here to download high resolution image](#)



Figure



58°30'W

58°0'W

57°30'W

83°30'S

83°50'S

Legend

● Be-10 exposure age

Grounding Line

Childs Glacier

Roderick Valley

Pillow Knob

Storey Peak

Teeny Rock

Williams Hills

Mt Hobbs

Pt 781

Pt 903

Foundation Ice Stream

McConnachie Rock

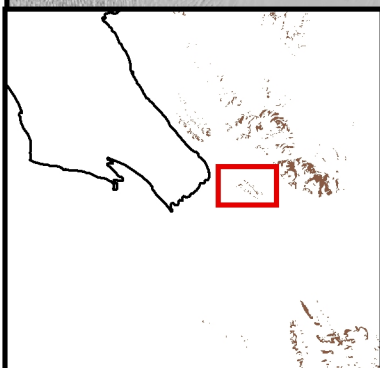
Academy Glacier

WIL-5 WIL-6
WIL-4 WIL-3
WIL-1 WIL-20 WIL-21
WIL-18 WIL-19

WIL-15 WIL-8
WIL-17 WIL-13

WIL-26 WIL-27

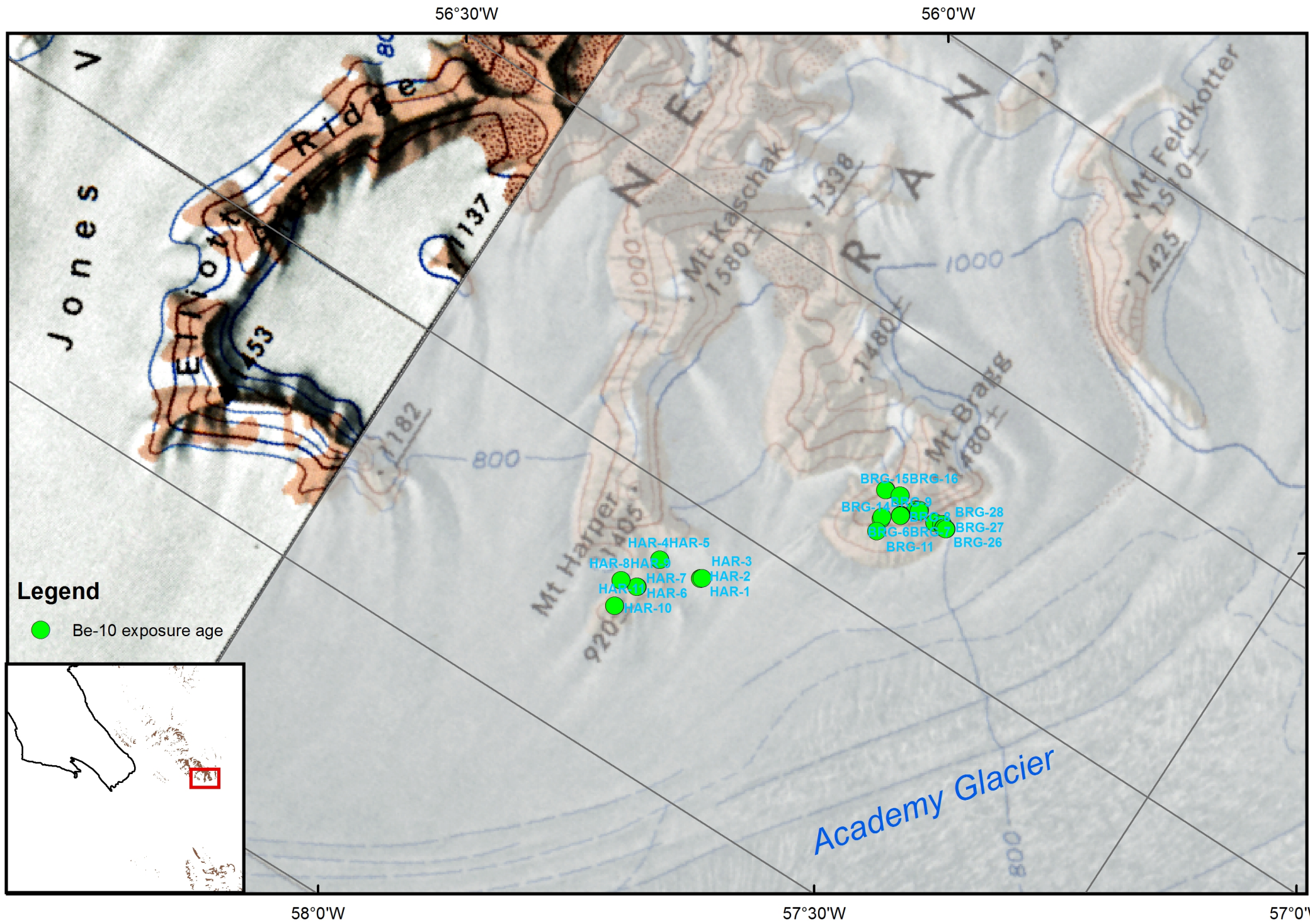
WIL-31 WIL-32 WIL-33
WIL-28



66°00'W

59°30'W

59°0'W

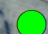


64°30'W

64°0'W

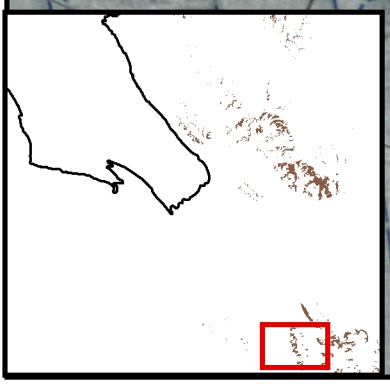
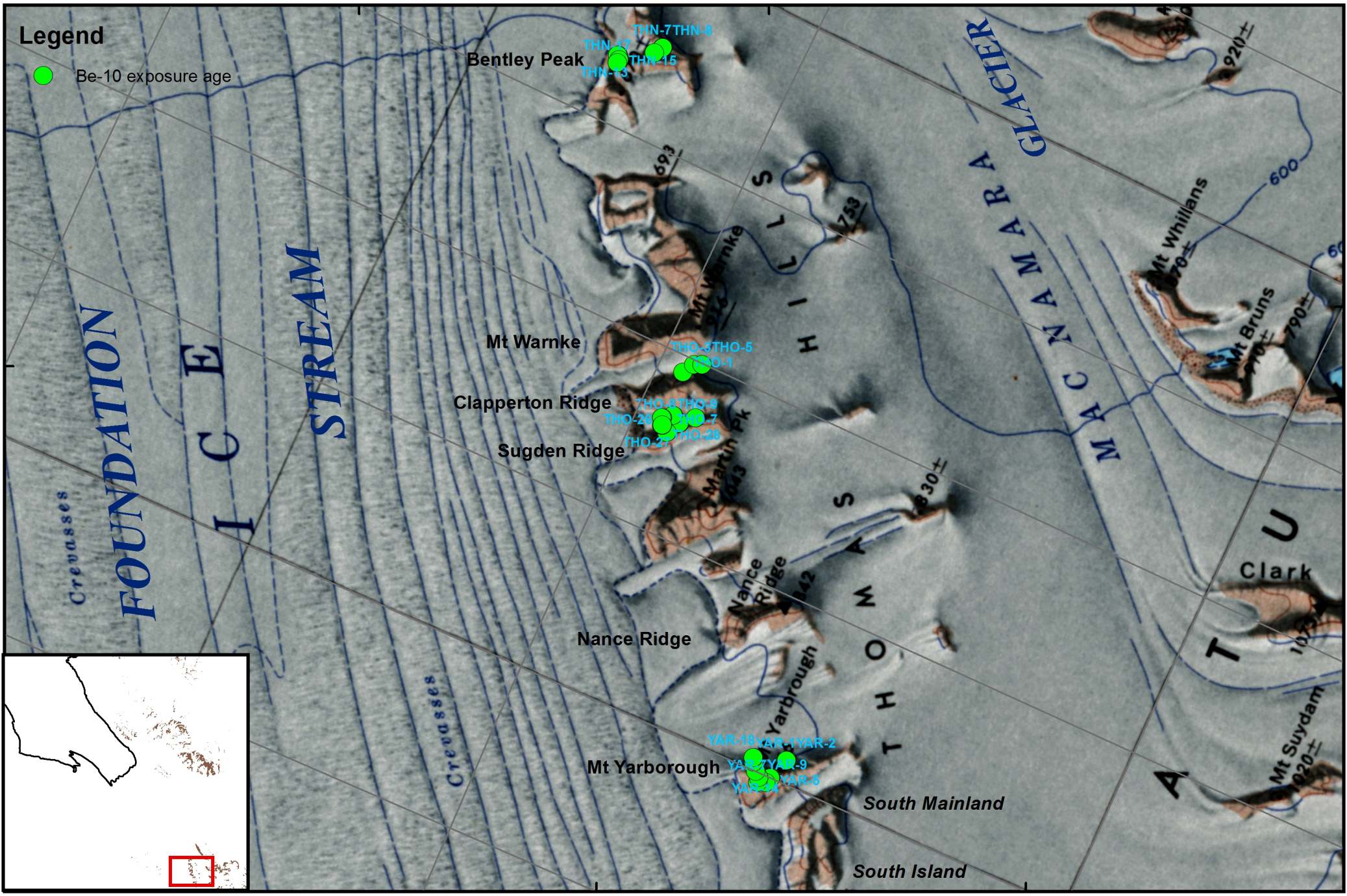
63°30'W

Legend

 Be-10 exposure age

84°10'S

84°30'S



67°0'W

66°30'W

66°0'W

South Mainland

South Island

Clark

Mt Suydam
1020±

Mt Bruns
790±

Mt Whillans
920±

MACNAMARA
GLACIER

THOMPSON
HILLS

Mt Warnke

Clapperton Ridge

Sugden Ridge

Nance Ridge

Mt Yarborough

Bentley Peak

Crevasses

FOUNDATION
ICE
STREAM

Figure

[Click here to download high resolution image](#)



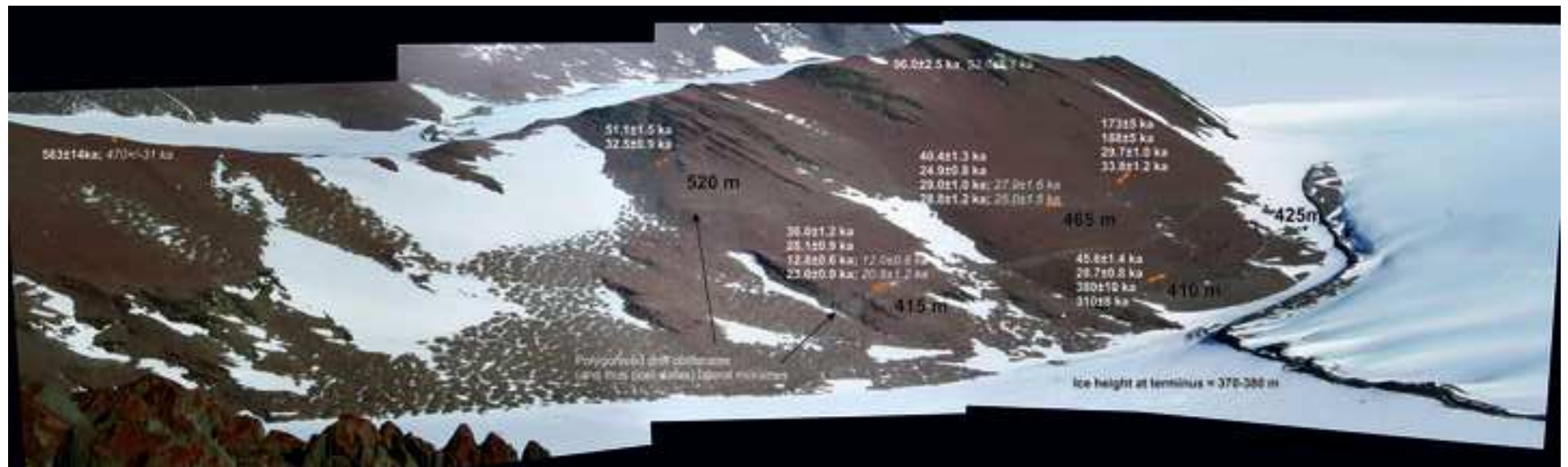
Figure

[Click here to download high resolution image](#)



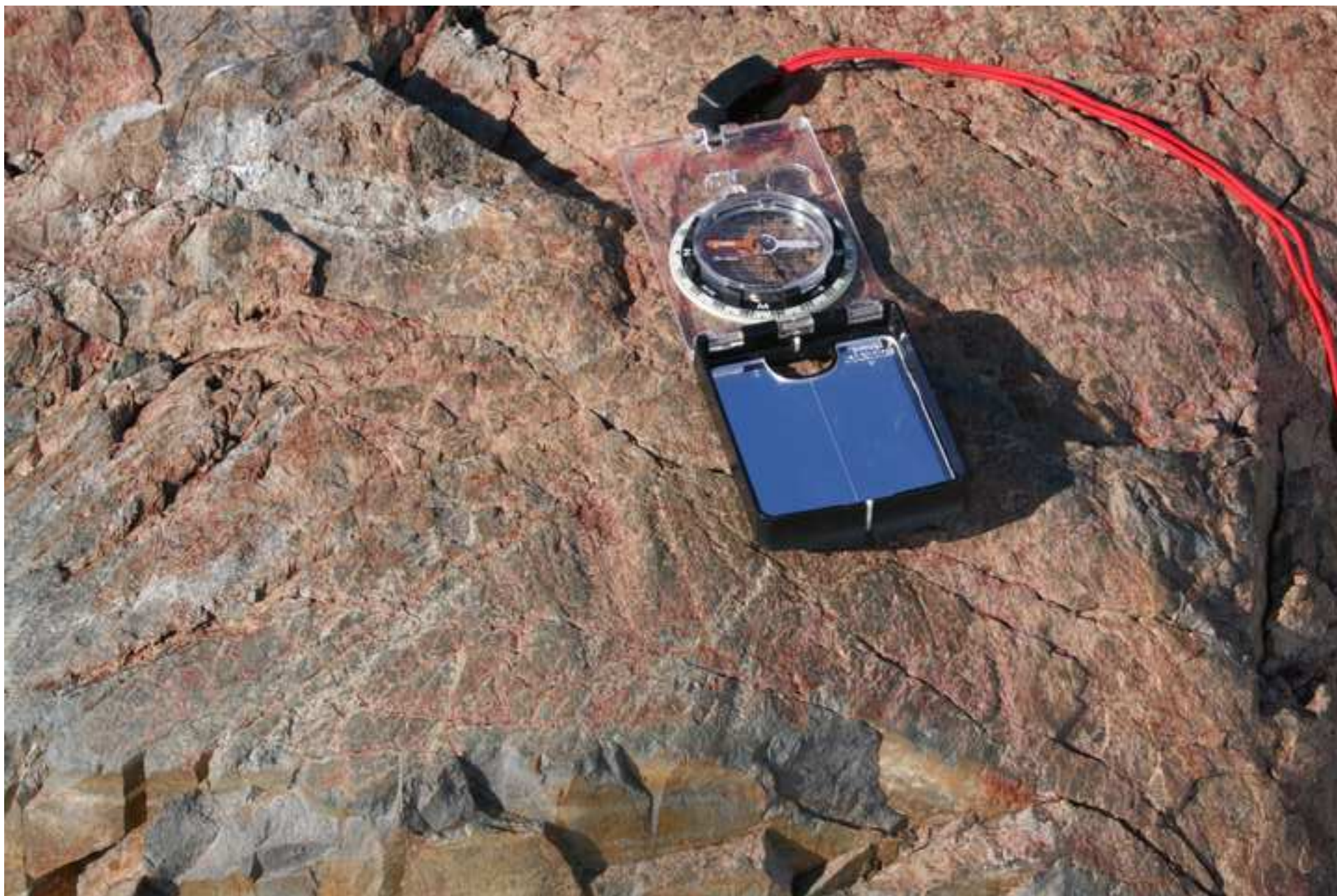
Figure

[Click here to download high resolution image](#)



Figure

[Click here to download high resolution image](#)



Figure

[Click here to download high resolution image](#)



Figure 4 revised

